DETERMINATION OF FATIGUE DAMAGE LEVEL OF GLASS FIBER REINFORCED EPOXY BASED NANOCOMPOSITES BY ELECTRICAL RESISTANCE CHANGE METHOD

Master's Thesis

Ömer KESKİN

Eskişehir 2024

DETERMINATION OF FATIGUE DAMAGE LEVEL OF GLASS FIBER REINFORCED EPOXY BASED NANOCOMPOSITES BY ELECTRICAL RESISTANCE CHANGE METHOD

Ömer KESKİN

Master's Thesis

Department of Advanced Technologies

Programme in Nanotechnology

Supervisor: Asst. Prof. Dr. Fatih TURAN

Eskişehir

Eskişehir Technical University

Institute of Graduate Programs

January 2024

This thesis was supported by the Scientific and Technological Research Council of Turkey (TUBITAK) under 1002 Program with the Grant No: 122M232

FINAL APPROVAL FOR THESIS

This thesis titled DETERMINATION OF FATIGUE DAMAGE LEVEL OF GLASS FIBER REINFORCED EPOXY BASED NANOCOMPOSITES BY ELECTRICAL RESISTANCE CHANGE METHOD has been prepared and submitted by Ömer KESKİN in partial fulfillment of the requirements in "Eskişehir Technical University Directive on Graduate Education and Examination" for the Degree of Master's in Advanced Technologies Department has been examined and approved on 17/01/2024.

Committee Members		**Title, Name and Surname**	**Signature**
Member	:	Asst. Prof. Dr. Fatih TURAN	
Member	:	Prof. Dr. Uğur SERİNCAN	
Member	:	Asst. Prof. Dr. Resul ÖZDEMİR	

Prof. Dr. Semra KURAMA
Director of the Institute of Graduate Programs

17/01/2024

SUPERVISOR APPROVAL

Master's student Ömer KESKİN, whom I supervise, has completed this thesis titled DETERMINATION OF FATIGUE DAMAGE LEVEL OF GLASS FIBER REINFORCED EPOXY BASED NANOCOMPOSITES BY ELECTRICAL RESISTANCE CHANGE METHOD. According to my inspections, the work is scientifically and ethically appropriate for the student to the thesis defense exam.

Supervisor

Asst. Prof. Dr. Fatih TURAN

ABSTRACT

DETERMİNATİON OF FATİGUE DAMAGE LEVEL OF GLASS FİBER REİNFORCED EPOXY BASED NANOCOMPOSİTES BY ELECTRİCAL RESİSTANCE CHANGE METHOD

Ömer KESKİN

Department of Advanced Technologies

Programme in Nanotechnology

Eskişehir Technical University, Institute of Graduate Programs, January 2024

Supervisor: Asst. Prof. Dr. Fatih TURAN

The purpose of this thesis is to monitor the damage level of fiber reinforced composites (FRPs) subjected to fatigue loading by using the electrical resistance change method and to prevent fatigue failures of FRPs by obtaining an electrical resistance change value with 95% reliability using Weibull analysis. Thus, it is aimed to develop a method to reduce the economic and safety risks of FRPs caused by fatigue damage.

First, the woven glass fiber reinforced epoxy composite laminates were manufactured by vacuum bagging method. Multi walled carbon nanotubes (MWCNTs) were employed as filler materials to obtain electrical conductivity in composites. The distribution of MWCNTs in epoxy matrix was achieved by ultrasonication. Then, tensile strength of composites was determined by conducting static tensile tests. In-situ damage monitoring of composite specimens during fatigue tests by electrical resistance change method was carried out. Finally, Weibull analysis was applied to obtain a critical electrical resistance change ratio with % 95 reliability to be used as a reference value to prevent FRP composites from fatigue failures.

Fatigue tests were conducted at two different stress amplitudes. The critical cycles at the fatigue failure and the corresponding critical electrical resistance change value for two different stress amplitudes were determined. An electrical resistance change value with 95% reliability using Weibull analysis was obtained to prevent fatigue failure for a particular stress amplitude.

Keywords: Composite materials, Fatigue test, Damage monitoring, Electrical resistance change method, Weibull analysis.

ÖZET

CAM ELYAF TAKVİYELİ EPOKSİ MATRİSLİ NANO KOMPOZİTLERİN YORULMA HASAR SEVİYESİNİN ELEKTRİKSEL DİRENÇ DEĞİŞİM YÖNTEMİYLE TESPİT EDİLMESİ

Ömer KESKİN

İleri Teknolojiler Anabilim Dalı Anabilim Dalı

Nanoteknoloji Bilim Dalı

Eskişehir Teknik Üniversitesi, Lisansüstü Eğitim Enstitüsü, Ocak 2024

Danışman: Dr. Öğr. Üyesi Fatih TURAN

Bu tezde, yorulmaya maruz kalan FRP yapılarda, yorulma sonucu oluşan hasarların elektriksel direnç değişim yöntemiyle eş zamanlı olarak izlenebilmesi ve Weibull analizi ile yorulma hasarlarını önleyebilecek yüksek güvenirlikli kritik bir elektriksel direnç değişim oranının tespit edilmesi amaçlanmıştır. Böylece FRP yapılarda yorulmaya bağlı ekonomik ve güvenlik anlamında oluşabilecek risklerin minimuma indirgenmesi için bir metodun geliştirilmesi düşünülmüştür.

İlk aşamada, proje kapsamında cam elyaf takviyeli epoksi kompozit numuneler vakum torbalama yöntemiyle üretildi. Kompozit malzemeler içerisinde elektriksel iletkenliğin elde edilebilmesi için çok duvarlı karbon nanotüp dolgu malzemesi olarak kullanıldı. Nanopartiküllerin epoksi içerisinde dağılımı ultrasonikasyon yöntemi ile yapıldı. İkinci aşamada, üretimi yapılan kompozit numunelerin statik olarak uygulanacak çekme testi ile çekme mukavemetleri elde edildi. Statik testlerden elde edilen veriler kullanılarak kompozit malzemelerin yorulma testleri ve eş zamanlı elektriksel direnç ölçümü yapıldı. Son aşamada, iki farklı gerilme genliğinde yorulma testleri yapıldı. Yorulma testleri ile iki farklı genlik için hasar anındaki çevrim sayıları ve bu çevrim sayılarına karşılık gelen kritik elektriksel direnç değişim oranları tespit edildi. Weibull analizi ile her bir genlik için o genlikteki yorulma hasarını önleyici %95 güvenirlikli kritik elektriksel direnç değişim oranı elde edildi

Anahtar Sözcükler: Kompozit malzemeler, Yorulma testi, Hasar izlemesi, Elektriksel direnç değişim yöntemi, Weibull analizi.

ACKNOWLEDGEMENTS

I would like to express my sincere gratitude to my supervisor, Dr. Fatih Turan, for his support and tireless effort in guiding me towards achieving my Master degree. I also would like to thank all my family members, who were always a source of inspiration for me in accomplishing this work.

I am gratefull to The Scientific and Technological Research Council of Turkey (TUBITAK) for the financial support under the grant number: 122M232.

Ömer KESKİN

17/01/2024

STATEMENT OF COMPLIANCE WITH ETHICAL PRINCIPLES AND RULES

I hereby truthfully declare that this thesis is an original work prepared by me; that I have behaved in accordance with the scientific ethical principles and rules throughout the stages of preparation, data collection, analysis and presentation of my work; that I have cited the sources of all the data and information that could be obtained within the scope of this study, and included these sources in the references section; and that this study has been scanned for plagiarism with "scientific plagiarism detection program" used by Eskişehir Technical University, and that "it does not have any plagiarism" whatsoever. I also declare that, if a case contrary to my declaration is detected in my work at any time, I hereby express my consent to all the ethical and legal consequences that are involved.

Ömer KESKİN

CONTENTS

Page

LIST OF TABLES

Page

LIST OF FIGURES

Page

GLOSSARY OF SYMBOLS AND ABBREVIATIONS

α	:	Characteristic Life
β	:	Shape Parameter
σ_{max}	:	Maximum Stress
σ_{min}	:	Minimum Stress
σ_{ult}	:	Ultimate Tensile Strength
ε_{max}	:	Maximum Strain
ε_{min}	:	Minimum Strain
ΔR	:	Resistance Change
CNT	:	Carbon Nanotube
ERC	:	Electrical Resistance Change
E_{loss}	:	Stiffness Loss
E_i	:	Stiffness at i^{th} Cycle
E_0	:	Initial Stiffness
FRP	:	Fiber Reinforced Polymers
MR	:	Median Rank
MWCNT	:	Multi-walled Carbon Nanotube
N	:	Cycle Number
N (%)	:	Fatigue Life
PAN	:	Polyacrylonitrile
R	:	Stress Ratio
S	:	Stress Amplitude
W	:	Watt

1. INTRODUCTION

Fiber-reinforced polymer-based composites can be subjected to fatigue due to dynamic loads in operating conditions. As a result of fatigue, damage mechanisms such as delamination, fiber fractures, matrix cracks, and fiber-matrix separations can occur within these structures. These damage mechanisms, invisible to the naked eye, can lead to the sudden failure of the composite structure, disrupting its structural integrity and resulting in unfortunate consequences in terms of safety and economy. Therefore, monitoring the structural integrity of composite materials is a crucial problem.

Various non-destructive testing methods have been developed and used for over two decades to inspect the integrity of composite materials. Methods such as ultrasonics, laser vibration, acoustic emission, X-ray, eddy current, and thermal wave mapping are among the most important non-destructive testing methods used to inspect and detect damage mechanisms such as fiber fractures and delamination. However, these methods are expensive and time-consuming, and they often require inspections that are not feasible under operational conditions. Critical damages, on the other hand, tend to occur during operational conditions.

To address the drawbacks of non-destructive testing methods, various techniques have been developed under the general term "structural health monitoring," providing a way to inspect damage in operational conditions. This allows for the continuous and frequent monitoring of damage mechanisms within composite materials. Vibration analysis, piezoresistive strain gauges, fiber optics, piezoelectric sensors, stress wave propagation methods, and piezoresistive micro carbon fibers are included in this group. While these methods are to some extent successful, each has its own disadvantages. Generally, they require a considerable number of sensors, lack sensitivity for small damages, and may disrupt material integrity due to the need for integration with the composite material.

Carbon nanotubes (CNTs) dispersed within polymer matrix materials can be utilized as piezoresistive sensors to control deformations and damage mechanisms occurring in composite materials. CNTs, known for their excellent electrical conductivity, create an electrical resistance within the composite material when distributed in a network structure within the matrix material. Mechanical deformation applied to the material leads to disruption in the network structure of the dispersed CNTs and a decrease in contact points between CNTs, causing an increase in the material's resistance. Consequently,

electrical resistance becomes a function of the applied deformation, allowing the tracking of deformation and, depending on the deformation, the amount of damage under operational conditions.

Moreover, the increasing commercial applications of CNTs enable them to be used as a contributory material in improving the properties of fiber-reinforced composites due to their superior mechanical, thermal, and thermal properties. While CNTs serve as a natural sensor in damage detection due to their excellent electrical conductivity, their superior mechanical properties allow them to enhance the toughness and structural performance of the polymers they are incorporated into.

In this thesis, the aim is to detect fatigue damage in multi-walled carbon nanotube (MWCNT) filled woven glass fabric-reinforced epoxy-based composite materials subjected to fatigue at different amplitudes under tension-tension mode using the electrical resistance change (ERC) method. In addition, high-reliability electrical resistance change value, which can be used as a preventative, reference value for fatigue damage is statistically determined using Weibull analysis.

The first section of the thesis includes a literature review and general information related to the research topic. This section covers the advantages, manufacturing, and application area of fiber reinforced composite materials. The general concept of damage sensing of composites by electrical resistance change method is reviewed by giving examples from the literature. Subsequently, general information about fatigue damage in composite materials and fatigue tests is provided, followed by a discussion of the Weibull reliability analysis, an important statistical approach in fatigue life analysis.

The Materials and Methods section discusses the materials used in the thesis and provides information on the applied production methods and the methodology of the implemented test procedures. This includes the distribution procedure of nanoparticles in epoxy (particularly ultrasonication), the production methods of MWCNT-filled fiber-reinforced epoxy composites, fiber-reinforced epoxy composites. Additionally, this sectioim covers the electrical conductivity measurement procedure, static tensile test, and fatigue test procedures.

In the Results section, the outputs obtained from experiments are discussed by presenting them graphically. The effect of ultrasonication duration and power and MWCNT concentration on the electrical properties of epoxy are examined to determine the optimum ultrasonication parameters for dispersion. The electrical resistance

measurements of glass fiber reinforced composites are measured to find the optimum MWCNT concentration for damage sensing during fatigue testing. The static tensile test results and the fatigue test results are demonstrated. Simultaneous electrical resistance measurements of composite specimens are performed during fatigue tests. Electrical resistance change characteristics of composites at two different stress amplitudes during fatigue tests are presented. In the final stage, the electrical resistance change values obtained at two different stress amplitudes are employed for Weibull analysis. The electrical resistance changes corresponding to 95%, 80%, and 50% Weibull reliability was determined.

2. LITERATURE REVIEW

2.1. Fiber Reinforced Composites

Composite materials consist of two or more phases on a macroscopic scale, whose mechanical properties and performance are designed to be superior to those of the constituent materials acting independently (Daniel & Ori Ishai, 2006). One of the phases, called reinforcement, is stiffer and stronger, whereas the other phase, called matrix is the less stiff and weaker. In addition, the distinct phase between the reinforcement and the matrix is known as interphase. The properties of composite materials depend on the properties of the constituents, their geometry, and the distribution of the phases. One of the most important parameters is the volume fraction of the reinforcement. The higher the volume fraction of the reinforcement, the greater the mechanical performance of the composite material. In the case of low – to medium performance composite materials, the reinforcement phase is usually in the form of short fiber that provides limited reinforcing and stiffening effect. In the case of high-performance structural composites, the continuous form of reinforcement fibers provide high stiffness and mechanical strength in the fiber direction. The matrix phase on the other hand, provides protection for the sensitive fibers, supports the fibers in a particular shape, and transfers the applied stress to the fibers.

The composite materials are classified into three broad categories depending on the type, geometry, and orientation of the reinforcement phase as shown in Figure 2.1. Particulate composites consist of particles of various sizes and shapes randomly dispersed within the matrix. Because of the usual randomness of particle distribution, these composites can be regarded as quasi-homogeneous and quasi-isotropic on a scale much larger than the particle size and spacing (macro scale). Discontinuous or short fiber composites contain short fibers, nanotubes, or whiskers as the reinforcing phase. These short fibers can be either all oriented along one direction or randomly oriented. Continuous fiber composites are reinforced by long continuous fibers and are the most efficient from the point of view of stiffness and strength. The continuous fibers can be all parallel in unidirectional fiber reinforced composites, can be oriented at right angles to each other in cross-ply or woven fabric reinforced composites, and can be oriented along several directions in multidirectional fiber reinforced composites.

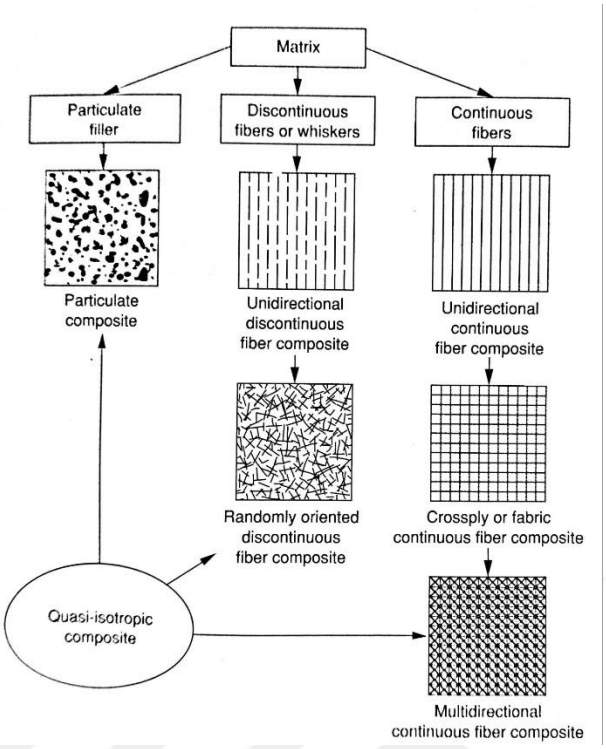

Figure 2.1. *Classification of composite material systems.*

In continuous fiber reinforced composites each layer is called a lamina. A lamine is an orthotropic material with principal material axes in the direction fibers (longitudinal), normal to the fibers in the plane of the lamina (in-plane transverse), and normal to the plane of the lamina. The structure made up of two or more layers (laminae) stacked together at various orientations is called laminate. The layers can be of various thicknesses and consist of different materials. Figure 2.2 illustrates the different scale of a laminated composite.

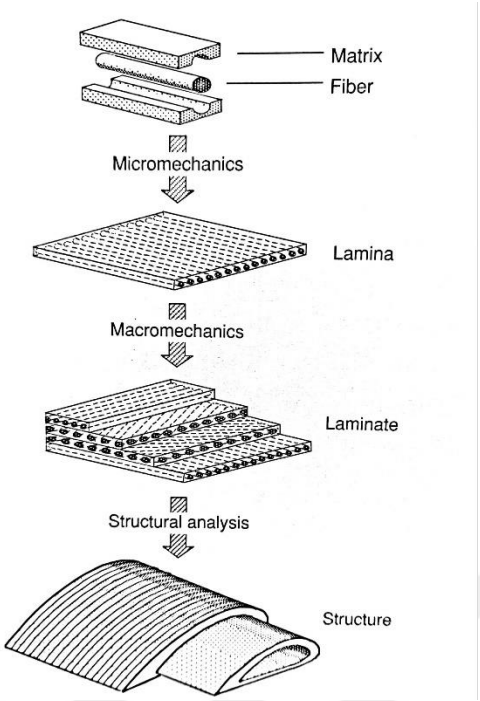

Figure 2.2. The scale of composite materials.

A large variety of fibers are available as reinforcement for composites. The desirable characteristics of most reinforcing fibers are high strength, high stiffness, and relatively low density. Each type of fiber has its own advantages and disadvantages as listed in Table 2.1. The mechanical properties of some fibers are also given in Table 2.2. Glass fibers are the most commonly used in low – to – medium performance composites because of their high tensile strength and low cost. They are limited in high performance composite applications because of their relatively low stiffness, low fatigue endurance, and rapid property degradation with exposure to severe hygrothermal conditions. Glass fibers are produced by extrusion of a molten mixture of silica (SiO_2) and other oxides through small holes of a platinum alloy. A coupling agent, or sizing, is applied to the fibers to protect their surface and ensure bonding to the resin matrix. An assembly of collimated fibers is called a yarn or tow and a group of collimated yarns is called a roving. Since the glass fibers are isotropic, they have isotropic properties.

Table 2.1. *Advantages and disadvantages of reinforcing fibers.*

Fiber	Advantages	Disadvantages
Glass	High strength Low cost	Low stiffness Short fatigue life High temperature sensitivity
Aramid	High tensile strength Low density	Low compressive strength High moisture absorption
Carbon	High strength High stiffness	High cost
Boron	High stiffness High compressive strength	High cost
Ceramic (Silicon carbide, alumina)	High stiffness High use temperature	Low strength High cost

Table 2.2. *Mechanical properties of some reinforcing fibers.*

Type	Density	Modulus (Gpa)	Tensile Strength (MPa)
Glass	2.54	73	3450
Carbon (T300)	1.76	230	3100
Graphite (T50)	1.67	390	2070
Boron	2.5	395	3450
Aramid	1.45	131	3800
Silicon carbide (Nicalon)	3.1	400	4140
Silica	2.19	73	5800

Carbon fibers are the most widely used for advanced composites and they are manufactured in many forms with a range of stiffness and strengths depending on the manufacturing process. Carbon fibers are manufactured from precursor organic fibers, such as rayon or polyacrylonitrile (PAN), or petroleum pitch. The detailed manufacturing method of carbon fibers can be found in elsewhere (Daniel & Ori Ishai, 2006).

Aramid fibers are organic fibers manufactured by dissolving the aromatic polyamide in sulfuric acid and extruding through small holes in a rotating device. Kevlar fibers have higher stiffness than glass fibers. Kevlar fibers have low density, about half that of glass, high tensile strength, and excellent toughness and impact resistance. However, Kevlar composites have very low longitudinal compressive and transverse tensile strengths and are sensitive to moisture absorption. Boron and other ceramic fibers are characterized by high stiffness, high use of temperature, and reasonably high strength.

They are not commonly used with polymeric matrices but rather with metal or ceramic matrices for high temperature applications. A comparative representation of some typical fibers from the point of view of specific strength and specific modulus is shown in Figure 2.3.

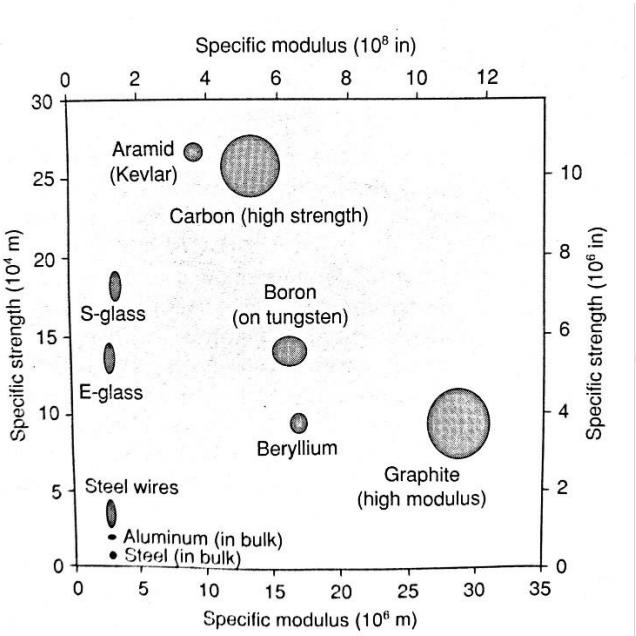

Figure 2.3. *Mechanical performance map of fibers used in structural composite materials.*

Fiber reinforced composites can also be classified based on the matrix type as following: polymer, metal, ceramic, and carbon. Polymer matrix composites include thermoset or thermoplastic resins reinforced with glass, carbon, aramid, and boron fibers. They are used primarily in relatively low temperature applications. Metal matrix composites consist of metals or alloys reinforced with boron, carbon, or ceramic fibers. They are best suited for very moderate temperature applications. Ceramic matrix composites consist of ceramic matrices reinforced with ceramic fibers and are used for very high temperature applications. Carbon composites consist of carbon or graphite matrix reinforced with graphite yarn or fabric. They have unique properties of relatively high stiffness and moderate or low strength at high temperatures coupled with low thermal expansion and low density.

Matrices are used in the following forms in composites as shown in Table 2.3: polymeric, ceramic, metallic, and carbon. The most extensively used matrices are polymeric, which can be thermosets or thermoplastics. The polymeric matrices are not suitable for high temperature applications. On the other hand, the other matrices are

considered for high temperature applications, with increasing use temperature from metallic to ceramic and carbon matrices.

Table 2.3. *The physical and mechanical properties of some matrices*

Property	Epoxy	Polyester	Vinylester	Polyimide	Poly-ether-ether ketone (PEEK)
Density (g/cm3)	1.17-1.28	1.1-1.5	1.15	1.4-1.9	1.32
Young's modulus (GPa)	3.4-4.3	3.2-3.5	3-4	3.1-4.9	3.7
Tensile strength (MPa)	69-90	40-90	65-90	70-120	96
Glass transition temperature (^{0}C)	150-300	50-110	-	280-320	143

Thermoset polymers are the most predominant types of matrix systems. Thermoset resins undergo polymerization and cross linking during curing with the aid of a hardening agent and heating. They do not melt upon reheating, but they decompose thermally at high temperatures. The most commonly used thermosets are unsaturated polyester, epoxies, polyimides, and vinyl esters. Polyesters are used in large quantities with glass fiber reinforcement for quick-curing and room temperature curing systems in a variety of commercial products such as automotive, boats, ships, storage tanks, and so on. Polyester matrix composites have good mechanical properties. The most highly developed of the thermoset polymers are epoxies of DGBEA type (diglycidyl ether of bisphenol A). They have better mechanical and thermal properties than polyesters. They can be formulated with a range of stiffness. Depending on the hardening agent, that is amine or anhydride, epoxies can be cured at different temperatures, typically 120 ^{0}C or 175 ^{0}C. The lower temperature curing epoxies are used in components exposed to low or moderate temperature variations. On the other hand, those cured at a higher temperature are used in high performance components exposed to high temperature and moisture variations. Vinylesters combine some of the desirable properties of both epoxy and polyester. They have fast and simple curing with good mechanical and thermal properties. Vinylester matrix composites are preferred in corrosive industrial and marine applications. Polyimides (PI) can be used in high temperature applications up to 300 ^{0}C. However, these polymers have relatively lower strength and more brittle at room temperature than epoxies. Table 4 lists mechanical and physical properties of typical thermoset polymers. Thermoplastics are fully polymerized polymers and can be altered physically by softening or melting them with heat. Thermoplastics used as matrices for composites include polypropylene (PP), poly-ether-ether-ketone (PEEk), polysulfone

(PS), and thermoplastic polyimides. They are more compatible with hot forming and injection molding fabrication methods. Compared to thermosets, thermoplastics can be processed more quickly and have much higher glass transition and maximum use temperatures up to 400 ^{0}C. They exhibit higher fracture toughness and are much less sensitive to moisture absorption. On the negative side, they exhibit temperature dependent behavior and shorter fatigue life.

Metal matrices are recommended for high temperature applications up to 800 ^{0}C. Commonly used metal matrices include aluminum, magnesium, and titanium alloys. Their use temperature is limited by the melting point. Ceramic and carbon matrices are used for higher temperature applications exceeding 1000 ^{0}C. They include glass, glass-ceramic, ceramic, and carbon matrices.

The manufacturing process of composite materials depends on their matrix types. For polymer matrix composites, a large number of fabrication methods are used as following:

- Hand lay up (open molding)
- Vacuum bag (Mallick, 2021a)
- Vacuum infusion (Spasojevic, 2019)
- Filament winding (Mantell & Springer, 1994)
- Fiber placement (Brasington et al., 2021)
- Pultrusion (Joshi, 2012)
- Resin transfer molding (Razali et al., 2021)

In general, autoclave is used after vacuum bag and vacuum infusion methods to cure the composite in a controlled way by the application of vacuum, heat, and pressure of inert gasses. Air is vacuumed out of the bag, heat and inert gas pressure cause the curing and densification of the material. Autoclave molding is used for fabrication of high-performance advanced composites for military, aerospace, transportation, marine, and infrastructure applications (Gupta et al., 2022).

Among the manufactured methods, vacuum bag method is used in this thesis. Vacuum bag molding is the primary composite manufacturing process for making laminated structures and is very common in the aerospace industry (Mallick, 2021b). It has limited use in the automotive industry since it is a labor-intensive process and may involve long cycle times. The starting material for the vacuum bag molding process is a prepreg that contains either unidirectional continuous fibers or a bidirectional fabric in a

partially cured (also called B-staged) thermosetting polymer, typically an epoxy. Plies of desired shape, size, and fiber orientation are cut from the prepreg roll and are stacked according to the design requirement, either by hand or by using a numerically controlled tape-laying machine. In some applications, the fibers are wet by hand which is called hand layup method. The stack is placed on the mold surface and is covered with a flexible polymer film, which serves as the vacuum bag (Figure 2.4). After sealing the vacuum bag around the edges, the assembly is placed either in an air-circulating oven or in an autoclave for curing. The application of vacuum removes air from the vacuum bag. The temperature in the oven or the autoclave is then raised at a controlled rate until the preset curing temperature is reached.

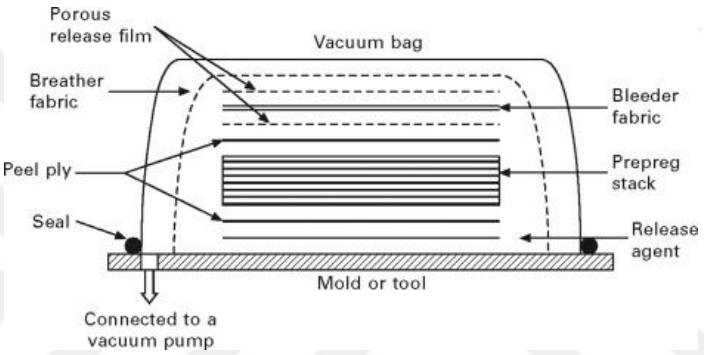

Figure 2.4. *Vacuum bag molding set-up* (Mallick, 2021c).

The high specific stiffness, the high specific strength, and excellent corrosion resistance make the composite materials ideal candidate for many applications such as aerospace, automotive, marine, energy, infrastructure, and biomedical applications. Aerospace structures, such as space antennae, mirrors, and optical instrumentation, make use of lightweight and extremely stiff composites. A very high degree of dimensional stability under severe environmental conditions can be achieved because these composites can be designed to have nearly zero coefficients of thermal and hygric expansion. In addition, composites are used in the other components of aircraft structures such as fairings, floorbeams, wing trailing edge surface, and the empennage. Composite materials, such as carbon/epoxy and graphite/titanium, account for approximately 50% of the weight of the Boeing 787, including most of the fuselage and wings. The Airbus A380 uses a substantial amount of composites, including a hybrid glass/epoxy/aluminum laminate, which combines the advantages an mitigates the disadvantages of metals and composites. The stealth characteristics of carbon/epoxy composites are highly desirable

in military aircraft structures. Small unmanned air vehicles are also made almost entirely of composites.

Composites are used in various forms in the transportation industry, including automotive parts and automobile, truck, and railcar frames. Transmission shafts, brake discs, and leaf springs are of example of automobile structures made of composite materials.

In marine industry, composites have many advantages such as insulation, lower manufacturing cost, low maintenance, and lack of corrosion. In the energy industry, carbon fiber composites have been used in blades of wind turbine generators that significantly improve power output at a greatly reduced cost. Biomedical applications of composites include prosthetic devices ad artificial limb parts. Sporting products include tennis rackets, bicycle frames, skis, and golf sticks.

In infrastructure applications composites are used to reinforce structural members against earthquakes, to produce structural shapes for buildings and bridges, and to produce pipes for oil and water transportation.

2.2. Fatigue in Composites

Fatigue occurs with the repeated loading of a machine part. The maximum number of cycles that a material can endure under repeated loads without experiencing fatigue damage provides the material's fatigue life under that load. It is known that fatigue strength is lower than the static strength of a material. This is because damage occurs and grows within the structure exposed to fatigue, leading to a reduction in mechanical properties (Reifsnider, 1991).

Unlike metals, composite materials are inhomogeneous (on a gross scale) and anisotropic. They accumulate damage in a general rather than a localized fashion, and failure does not always occur by the propagation of a single macroscopic crack. The micro-structural mechanisms of damage accumulation, including fibre breakage and matrix cracking, debonding, transverse-ply cracking, and delamination, occur sometimes independently and sometimes interactively, and the predominance of one or the other may be strongly affected by both materials variables and testing conditions.

Various factors influence the fatigue mechanism of composite materials such as stacking assembly of reinforcements, type of reinforcement, and their orientation, etc. The failures can be observed anywhere around the fiber-matrix interface, the matrix layers interfaces, and fibers (İTÜ tezde Jawaid et al., 2019). During the fatigue of fiber-

reinforced composite materials, changes occur in properties such as residual stress, elasticity modulus, strain, crack length, crack density, and the number of debonded fibers (Harris, 2003). In particular, the reduction in the modulus and strength occur as a result of fatigue (Hwang & Han, 1986). The repeating loading leading to fatigue causes micro-scale matrix cracks and fiber-matrix separations in fiber-reinforced composites, initiating damage within the composite structure. In the progressive stages of fatigue, fiber fractures and delamination occur. In the final stage of the fatigue loading, composite structure loses its integrity. Figure 2.5 illustrates the typical damage mechanisms observed in fiber-reinforced composite materials (Markus Sause, 2010; Mayuet et al., 2015; Mostafa et al., 2017; Wang et al., 2023). The failure mechanisms based on their scale is shown in Figure 2.6.

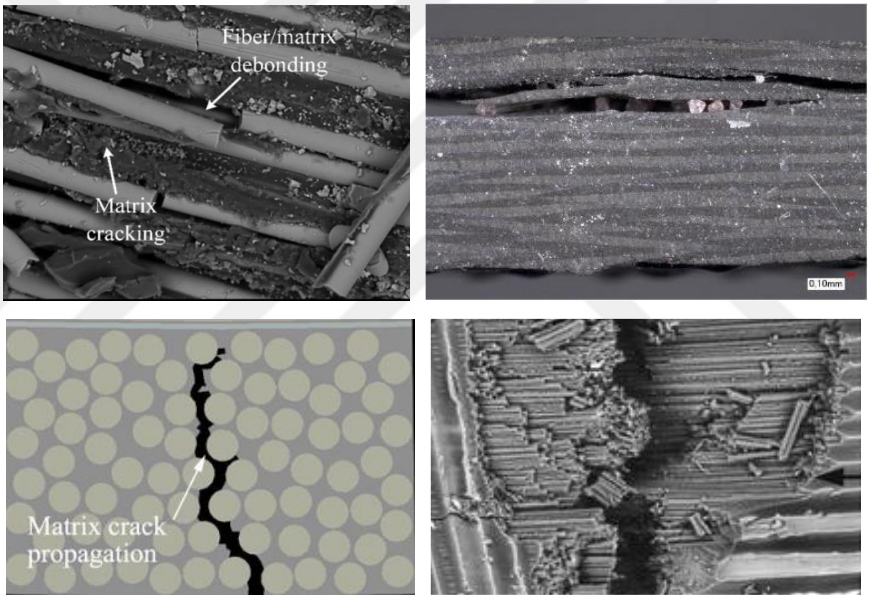

Figure 2. 5. *Typical damage mechanisms in fiber reinforced composites* (Markus Sause, 2010; Mayuet et al., 2015; Mostafa et al., 2017; Wang et al., 2023)

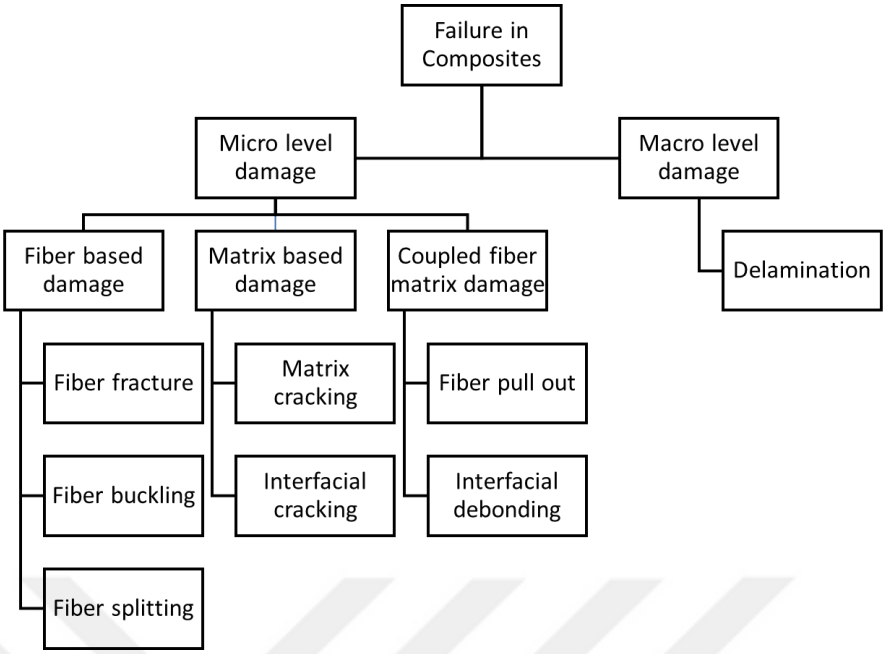

Figure 2.6. *The classification of failure mechanisms in fiber reinforced composites based on the failure dimension.*

2.3. Fatigue Testing

Fatigue tests are conducted using servo-hydraulic machines in two different control modes: displacement-controlled and load-controlled (Harris, 2003). In displacement-controlled fatigue tests, maximum and minimum displacements remain constant (Figure 2.7 (a)). As damage develops due to fatigue, the stiffness of the test specimen decreases over time. Consequently, the applied load required for constant displacement amplitudes decreases over time. In load-controlled fatigue tests, maximum and minimum applied loads remain constant (Figure 2.7 (b)). Due to fatigue-induced damage causing a loss of specimen stiffness, the displacement values corresponding to maximum and minimum loads decrease over time.

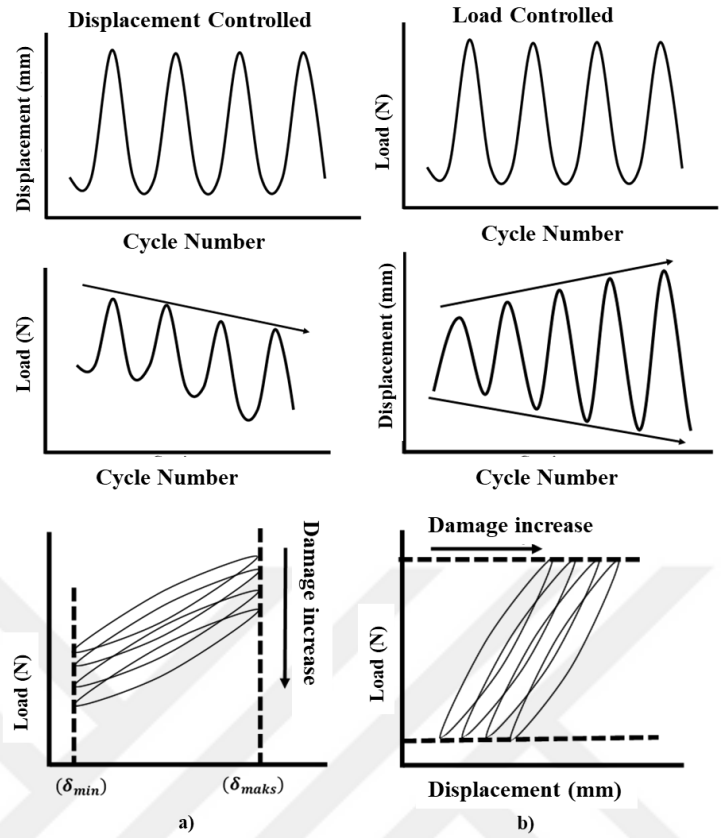

Figure 2.7. *a) The displacement controlled and b) load controlled fatigue tests*

In fatigue tests, load is applied to the test specimen sinusoidally with a constant frequency and amplitude (Figure 2.8). The obtained data is then graphically represented by converting it into displacement-cycle number or stress-cycle number curves. The parameter denoted by X in Figure 2.8 represents stress for load-controlled tests and displacement for displacement-controlled tests. Xmax, Xmin, and Xm represent the maximum, minimum, and mean stress or displacement, respectively during a fatigue test.

In a load-controlled fatigue test, the constant ratio of minimum and maximum stress is known as the stress ratio R for different values of the peak stress as represented in (2.1).

$$R = \sigma_{min}/\sigma_{max} \tag{2.1}$$

The R value indicates the type of fatigue test. In Figure 2.15, the cycle types corresponding to different R values are as follows(Harris, 2003):

1. Compression – compression cycle
2. Zero – compression cycle
3. Compression dominated alternating cycle
4. Fully reversed cycle
5. Tension dominated alternating cycle

6. Zero – tension cycle
7. Tension – tension cycle

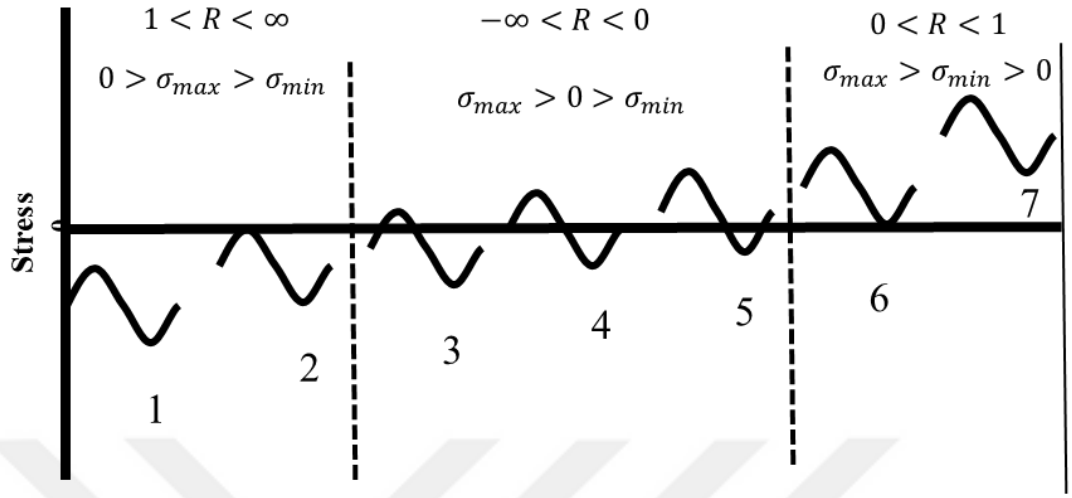

Figure 2.8. *Cycle types for different R values*

2.4. Weibull Analysis

Due to the inherent anisotropic nature of fiber-reinforced composite materials, there can be a broad distribution in static and dynamic test results. Additionally, variations in production quality constitute a factor that introduces differences in fatigue test results. It is well-known, especially in the case of composite materials, that the data obtained from fatigue tests exhibit a wide distribution. Given their frequent use in components exposed to fatigue during operation, such as aircraft wings, wind turbines, and leaf springs, reliability analyses hold significant importance for composite materials. Consequently, numerous studies focus on the Weibull analysis of composite materials, aiming to characterize their static and dynamic behaviors and determine fatigue lifetimes with a specified level of reliability (Ding & Cheng, 2021; Sakin & Ay, 2008a; Strzelecki, 2021).

Weibull distribution has been widely used to evaluate the fatigue data reliability in composite structures (Sakin & Ay, 2008b). Weibull analysis can be implemented using two or three-parameter distribution functions (Castillo & Canteli, 2009). In this study, two parameter distribution function was employed due to its simplicity and reliability. The probability density function of two parameter distribution is expressed in (2.2)

$$f(x) = \frac{\beta}{\alpha}\left(\frac{x}{\alpha}\right)^{\beta-1} e^{-\left(\frac{x}{\alpha}\right)^{\beta}} \qquad \alpha \geq 0,\ \beta \geq 0 \tag{2.2}$$

where α and β is the scale and shape parameters, respectively. α represents the characteristic life and β is the Weibull slope. The Weibull cumulative frequency function can be obtained by integrating the two sides of (2.2)

$$F(x) = 1 - e^{-\left(\frac{x}{\alpha}\right)^{\beta}} \quad (2.3)$$

where $F(x)$, and x is the probability of failure and variable, respectively.

Probability of survival $(R(x))$ can be obtained from (2.4);

$$R(x) = e^{-\left(\frac{x}{\alpha}\right)^{\beta}} \quad (2.4)$$

(2.3) can be linearized as (2.5) by taking double logarithm of both sides.

$$\ln\left(ln\left(\frac{1}{1-F(x)}\right)\right) = \beta lnx - \beta ln\alpha \quad (2.5)$$

(2.5) now becomes a linear function in the form of $Y = mX + c$ by setting,

$Y = ln\big(ln(1/1 - F(x))\big)$, $m = \beta$, and $c = -\beta \ln(\alpha)$.

The following procedure needs to be followed to obtain the shape parameter (α) and the Weibull slope (β) for drawing Weibull lines:

1. The electrical resistance change values (ΔR_i) corresponding to fatigue failures for each type of samples in ascending order are sorted.

2. Bernard's Median Rank Formula is used to obtain median life (50% failure probability) for each value using (2.6).

$$MR_i = \frac{i-0.3}{n+0.4} \quad (2.6)$$

where i and n represents the serial number and the total number of electrical resistance change value as percentage at the failure, respectively.

3. The values of Y axis in Weibull line are calculated by $ln\big(ln(1/1 - MR_i)\big)$.

4. The values of X axis in Weibull line are calculated by $\ln(\Delta R_i)$.

5. The Weibull line is drawn and the slope of Weibull line (β) and the c values are obtained by linear regression.

6. α values are obtained by $c = -\beta \ln(\alpha)$.

7. Rearranging (2.4), the $R(x) - \Delta R$ survivability graph can be drawn using (2.7) as following:

$$\Delta R = \alpha.(-lnR(x))^{1/\beta} \quad (2.7)$$

2.5. Electrical Resistance Change Method

Cracks in metals typically initiate from the material's surface and propagate visibly throughout its thickness. In composite materials, however, damage detection is challenging. This is because damage mechanisms, such as delamination and fiber breakage, occur within the composite structure, and the damage is often not visible on the

surface. This, in turn, compromises the structural integrity of the composite, leading to adverse consequences in terms of safety and economy (Raulo et al., 2016). Therefore, non-destructive internal inspections are crucial for detecting small damages within composite materials.

Many non-destructive testing methods have been developed and utilized for over 20 years to assess the integrity of composite materials. For instance, methods such as ultrasonics, laser vibration, acoustic emission, X-ray, eddy current, and thermal wave mapping are among the most important non-destructive testing techniques used to monitor and detect damage mechanisms such as fiber breakage and delamination (Mazela et al., 2020). However, these methods are both expensive and time-consuming, requiring the examination for damage detection to take place when the structure is not in operational condition. Critical damages, on the other hand, often occur during operational conditions. To address the disadvantages of non-destructive testing methods, several techniques have been developed that eliminate these drawbacks. Referred to as structural health monitoring, these methods provide a damage inspection technique under operational conditions (Abot et al., 2010). Thus, damage mechanisms within composite materials can be monitored frequently and continuously. Vibration analysis, piezoresistive strain gauges, fiber optic and piezoelectric sensors, stress wave propagation methods, and piezoresistive micro carbon fibers are included in this category. Although these methods are to some extent successful, each has its own disadvantages. In general, these methods typically require a significant number of sensors, lack sensitivity for small damages, and, due to the need to integrate with composite materials, may compromise material integrity.

The concept of self-damage detection through the electrical resistance change method, where the composite structure itself acts as a sensor, helps eliminate these disadvantages. Damages occurring in the internal structure cause an increase in the electrical resistance of the composite structure. Monitoring this resistance change allows obtaining an idea about the integrity of the composite structure. When this method was first implemented, damage detection through the electrical resistance change method in carbon fiber-reinforced polymer composites was based on leveraging the electrical conductivity of carbon fibers. However, using carbon fibers as sensors allows the tracking of damage only when the conductive carbon fibers break. The breakage of carbon fibers occurs in the final stages of the composite structure's strength (Prakash, 1980). Damage such as matrix cracking in the insulating matrix medium and delamination damage

between layers cannot be sensed by carbon fibers. In glass fiber-reinforced composites, the structure is entirely insulating, making damage detection impossible through the electrical resistance change method. Therefore, to monitor all damage mechanisms, it is necessary to convert the insulating matrix material into a conductive one. One of the methods applied to make the matrix material conductive is the dispersion of highly conductive nanoparticles within the insulating matrix material to create electrically conductive network in the composite structure. For this purpose, one of the most common nanoparticles used is carbon nanotubes (CNTs) due to their excellent electrical conductivity (Dresselhaus et al., 1995; Ebbesen & Ajayan, 1992; Hamada et al., 1992). When CNTs are distributed in a network structure within the matrix material, they make the matrix material electrically conductive by contacting each other and tunnelling effect (Figure 2.9).

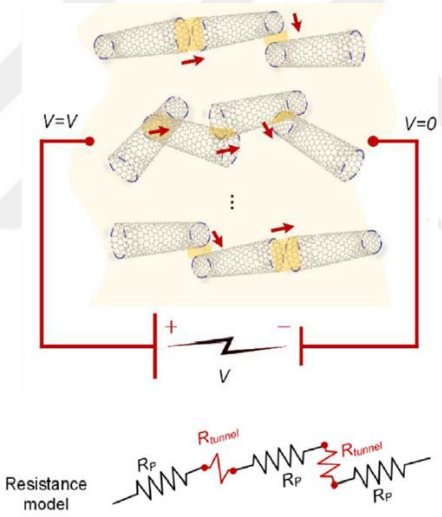

Figure 2.9. *Schematic representation of distributed CNT networks for resistance modelling*

The mechanical deformation under the applied loading causes the contact points, that provide electrical conductivity in the network structure, decrease and diminishes the tunneling effect due to the increased distance between CNTs (Figure 2.10). Therefore, electrical resistance becomes a function of the applied deformation, allowing the monitoring of the amount of deformation and, consequently, the extent of damage within the material under loading conditions.

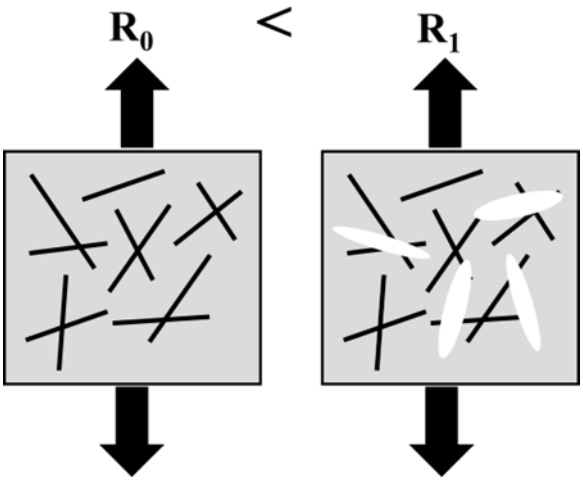

Figure 2.10. *The schematic representation of deformation mechanism of CNT network under tensile load*

.

Many studies have been conducted on the use of CNTs as damage detection sensors in fiber-reinforced composite materials. Simultaneous detection of damage modes such as matrix cracks, fiber fractures, and delamination between layers occurring due to static, repetitive, and impact loading in composite materials can be achieved through the electrical resistance change method.

It is widely recognized that damage initiation in composite laminates typically begins with failure modes dominated by the matrix, such as matrix cracking and delamination. This is subsequently followed by fiber breakage, which generally occurs toward the later stages of the composite material's lifespan. Some studies from the literature related to damage sensing using nanotubes as well as the different dispersion techniques of CNTs within the composites are reported below.

Thostenson & Chou, 2006 employed high shear mixing techniques, including calendaring and a three-roll mill, to disperse multi-walled carbon nanotubes (MWCNTs) within epoxy resin. This process established a percolating network to initiate and track damage evolution in glass fiber-reinforced polymers (GFRPs). They investigated the interlaminar delamination and transverse microcracking in unidirectional and cross-ply laminates, respectively. During the delamination tests there was a notable increase in electrical resistance when delamination initiated, and this resistance continued to rise progressively until the specimen eventually failed. On the other hand, in the context of microcracking detection, the electrical resistance exhibited a stepwise increase after the initiation of cracks. These distinct responses in sensing signals provided the opportunity to distinguish between various failure modes through the utilization of conductive carbon

nanotube networks. Böger et al., 2010) observed that the initial matrix crack occurring during tensile testing led to a significant change in resistivity, serving as an indicator for damage initiation. Gao et al., 2009 compared the acoustic emission (AE) method with the electrical resistance change method for the purpose of detecting damage in glass fiber-reinforced polymer composite. They used calendering approach to disperse CNTs within vinyl ether matrix. A strong correlation was observed between electrical resistance change data and the AE data during the initial loading phase. It was also observed that in elastic region of the loading no signal was detected whereas electrical resistance increased with applied load. This result indicates that ERC method is sensitive to strain although there is no crack inside the composite materials as opposed to the AE method in which the signals are emitted only if a damage occurs within the structure. Gao et al., 2011 investigated the effect of CNT concentration and dispersion level on damage sensing behavior of glass fiber composites under static and incremental tensile loading. The dispersion of CNTs within epoxy matrix was succeeded by three roll milling (calendering approach) with and without using sizing agent. It was found that sizing agent resulted in non-uniform CNT dispersion within epoxy causing degradation in the mechanical properties and the damage sensing sensitivity. This study highlights the importance of dispersion level effect on the damage sensing behavior. The homogeneous conductive network is desirable for efficient damage sensing property. electrical conductivity.

ERC method is also applicable to the composites which are exposed to cyclic loads to evaluate both the damage level and the failure stages during cycling loading. (Thostenson & Chou, 2008) investigated damage progression of glass/epoxy composites [0/90]s under cycling loading using dispersed CNTs in epoxy composites. The authors used calendaring technique for dispersion process of 0.5wt% CNTs in epoxy. A good correlation between the resistance and strain was found during cycling loading. The resistance / strain relation show hysteresis behavior due to the loading and unloading conditions throughout the tests. The study suggested that quantitative measure of damage level can be determined by investigating the resistance change curves that respond to mechanical damage.

Gao et al., 2009a reported the damage stages of glass/epoxy composites [0/90]s under cycling loading including matrix cracks and delamination using ERC method. The crack densities and residual elastic modulus were measured and correlated with the electrical resistance change.

ERC method is also used for sensing of damage level of composite plates under impact loading (Arronche et al., 2013; Loyola et al., 2013; Monti et al., 2011; Naghashpour & Van Hoa, 2013; Yesil et al., 2010; Zhang et al., 2015). Yesil et al., 2010 carried out a comparison study to investigate the effect of different CNT treatment methods on both the dispersion level and the impact damage sensing characterization by ERC method. The surface treatment of CNTs were achieved using hexamethylene diamine and nitric acid and two different surfactants: Triton X-100 and cetyl pyridinium chloride (CPC). The results showed that diamaine/CPC treatment exhibited better dispersion resulting in higher electrical resistance change sensitivity at impact loading. Gao et al., 2011 correlated the acoustic emission data with the electrical resistance change data of composite plates exposed to repeated impact loading. Naghashpour & Van Hoa, 2013 reported mapping technique for internal damage sensing of large composite plates under both the high-velocity and low-velocity impact.

Some studies have been conducted to structrural health monitoring of fiber reinforced composite materials under fatigue loading by ERC method using carbon nanoparticles. In general, the residual strain is the indication of damage state of composites in fatigue loading. Therefore, the ERC signal during fatigue loading with increasing cycle numbers can be compared with the residual strain to evaluate the integrity of composite structure. Yesil et al., 2010 observed that electrical resistance increased due to the accumulation of damage within composite, associated with the stiffness loss. Gao et al., 2010 investigated the damage stage of composites with various stacking sequence including $[0/90_2/0]$, $[0/90_3/0]$, $[0/90_4/0]$ by ERC method. It was shown that electrical resistance increased as a function of fatigue life. At first, significant increase in the resistance was observed in about 15% of fatigue life due to the crack initiation and accumulation. Then the linear increase in resistance was observed in about 80 % of fatigue life due to the delamination progression.

3. MATERIALS AND METHOD

In this thesis, the Duratek 1000 epoxy-based lamination resin system produced by the Duratek company was used as the polymer matrix material. The Duratek 1000 resin system consists of two components: the resin with the code DTE 1000 and the curing agent with the code DTS 1105, which allows for slow curing. Table 3.1 lists some physical properties of the Duratek 1000 resin system. The DTE 1000 and DTS 1105 components were mixed in a 1:4 ratio, according to manufacturer's recommendation. 2D woven glass fibres with an areal density of 200 g m^{-2} were used as reinforcement material in nanocomposite laminates. Multi-wall carbon nanotubes (MWCNTs) were used as carbon based nanoparticles for electrical conductivity in the epoxy composites. Table 3.2 lists some physical properties of MWCNTs.

Table 3.1. *The physical properties of Duratek 1000 epoxy resin system*

Property	**DTS 1000 + DTS 1105**
Density (g/cm^3)	1.1
Viscosity (mPas)	600
Pot life (min)	360

Table 3.2. *The physical properties of MWCNTs*

Property	**MWCNT**
Density (g/cm^3)	0.25
Surface area (m^2/g)	250-300
Particle size	diameter: 8-10 nm length: 10-30 µm

3.1. Ultrasonication

Ultrasonication is an effective method to disperse CNTs in liquids having a low viscosity, such as water, acetone, and ethanol. Since epoxy is in viscous liquid state, its viscosity is required to be reduced using a solvent such as acetone. In this study, no solvent was employed in the dispersion process of nanoparticles through ultrasonication to eliminate the residual solvent effect on the mechanical performance of nanocomposites for the purpose of obtaining reliable test data. Therefore, strong ultrasonication process

was performed at 150 W for 20 min to disperse the desired amount of nanoparticles in small amount of epoxy of 50 g as seen in Figure 3.1.

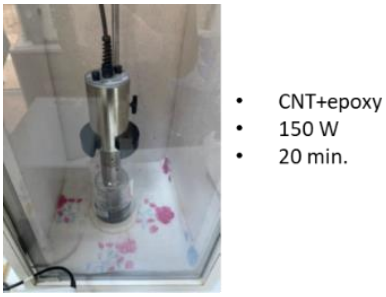

Figure 3.1. *Ultrasonication process*

3.2. Electrical Resistance Measurement

Since the dispersion quality of nanoparticles within a polymer is strongly dependent on both sonication power and time, we selected the optimum ultrasonication power and dispersion time based on the indirect measurement of dispersion quality. This was achieved by measuring the electrical resistance of 0.2 wt% CNT-filled epoxy mixtures that were dispersed at various ultrasonication powers and times. Rectangular specimens of about 70 mm in length, 10 mm in width, and 3 mm in thickness were molded for electrical resistance measurement as seen in Figure 3.2. Whiskered carbon fibers were used at both ends of the specimens to obtain good contact with the filler network in the specimen. Electrical resistance measurement was achieved using a LCR meter. Two batches with three specimens were prepared for consistency. The measured resistance values are the functions of the geometrical aspects of the specimens such as length and the cross-sectional area. Therefore, the measured resistance values were normalized to determine the specific electrical resistivity of the specimens using (3.1). In this equation, ρ, R, A, and L represent the specific resistivity, measured resistance, cross – sectional area, and length, respectively.

$$\boldsymbol{\rho} = \frac{\boldsymbol{RA}}{\boldsymbol{L}} \tag{3.1}$$

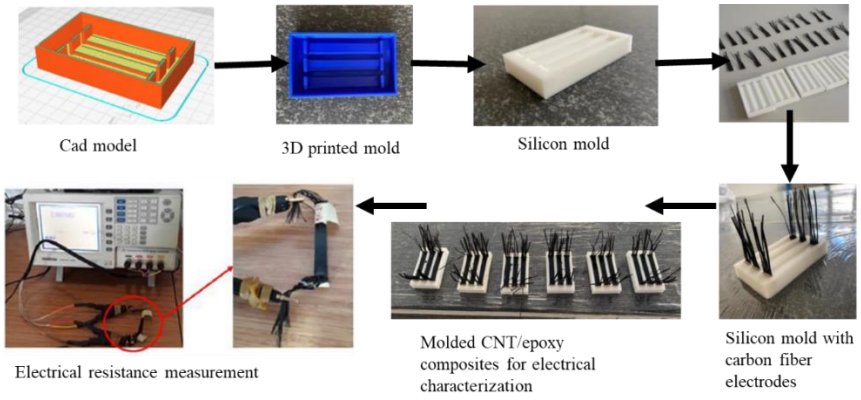

Figure 3.2. *Manufacturing steps of unreinforced specimens for electrical resistance measurement*

Glass/fiber reinforced epoxy composites should be electrically conductive for reliable damage sensing during fatigue loading so that the effect of MWCNT content on the electrical properties of glass fiber reinforced epoxy composites was measured to determine the optimum MWCNT content in epoxy composites. The electrical resistance of 0.1 % wt., 0.2 % wt., 0.3 wt., and 0.4% wt. MWCNT modified glass fiber reinforced epoxy composites were manufactured for this purpose.

3.3. Manufacturing of MWCNT Modified Glass Fiber Reinforced Epoxy Composites

Production of nanoparticle-filled glass fiber-reinforced composite samples was carried out using the vacuum bagging method. The vacuum bagging method is a low-cost and easily applicable technique, and the air voids resulting from manual layup are minimized. Thus, the composite structure becomes more robust. The application stages of the vacuum bagging method were conducted as follows:

- The surface of the mold, consisting of a 6 mm tempered flat glass plate, was waxed with a mold release wax. The purpose of this process is to facilitate the easy removal of the composite plate from the glass mold after production. For electrical resistance measurement, two different regions along the length of the plate were equipped with carbon fiber electrodes, positioned at equal distances from the center (Figure 3.3a). These carbon fiber electrodes enhance the contact surface with MWCNTs, thereby increasing the contact area and reducing contact resistance, ensuring accurate resistance measurements.
- The woven glass fibers, with dimensions of 250x250 mm, were laid onto the carbon fiber electrodes and impregnated with MWCNT filled epoxy resin using a

plastic spatula. The lamination process was repeated for a total of 10 layers of glass fibers (Figure 3.3b).

- The final layer of glass fiber was then placed parallel to the carbon fiber electrodes on the bottom surface (Figure 3.3c). Subsequently, peel ply and breather cloth were sequentially applied (Figure 3.3d). The peel ply fabric is used for easy removal of the composite material from the mold without sticking to the consumables on top of it. The breather cloth is used to absorb excess resin.
- After completing the entire molding process, the mold was enveloped with a vacuum bag using double-sided vacuum tape to create a vacuum-tight environment (Figure 3.3e).
- Finally, the mold was vacuumed using a vacuum pump (Figure 3.3e). After ensuring that there was no air leak in the mold, the composite plates were cured at the room temperature for one week.
- The cured composite plates were then cut into the rectangular specimens with the dimension of 250x2x2.5 mm for both fatigue testing and electrical resistance measurement (Figure 3.4a). The tabs made of woven glass fiber reinforced epoxy composites were glued at the ends on both sides of the specimens for the purpose of providing insulation between the electrically conductive grips and the specimens in order to obtain reliable resistance measurement during fatigue testing (Figure 3.4b). The tabs also prevents the composite specimens from localized damage by the grips. Figure 3.4c shows the schematic view of the rectangular composite specimens for the fatigue testing.

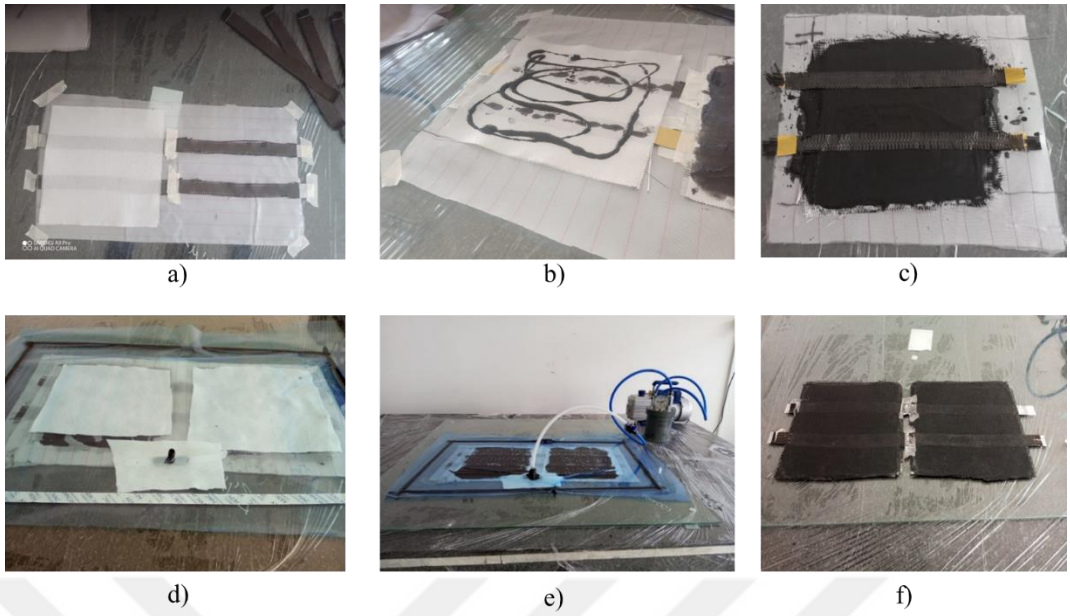

Figure 3.3. *Manufacturing steps of MWCNT filled glass fiber reinforced composite plates via vacuum bagging process.*

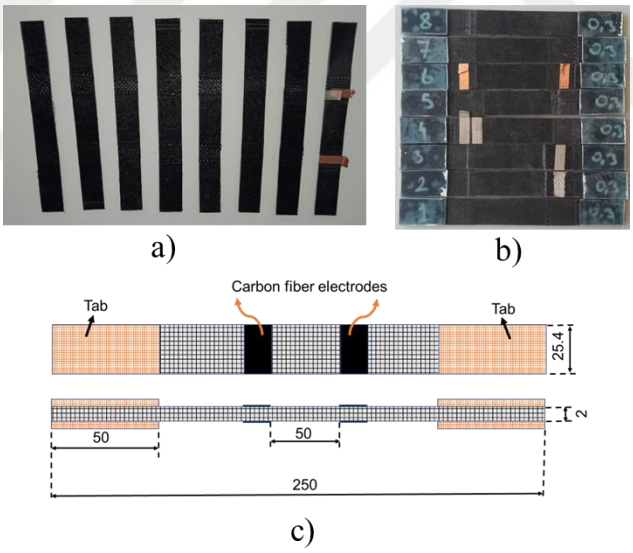

Figure 3.4. *Rectangular specimens a) with and b) without tabs and c) the schematic view of the rectangular specimens with the geometric details.*

3.4. Structural Health Monitoring by ERC Method in Fatigue Test

The purpose of the fatigue tests is to perform in-situ damage monitoring of glass fiber reinforced composites through simultaneous electrical resistance measurements during fatigue loading. Then, the electrical resistance change values of composites at failure due to fatigue can be detected for statistical analysis. During the test, the applied force and displacement amount can be obtained as raw data. Simultaneous electrical resistance measurements during the tests were conducted using a multimeter capable of

acquiring data at 10 Hz with carbon fiber electrodes on the top and bottom surfaces of the sample. To prevent the movement of the cables during the fatigue test, silver cloth pieces with high electrical conductivity were attached to both sides of the carbon fiber electrodes (Figure 3.5).

Figure 3.5. *The test setup for measuring electrical resistance change during fatigue test*

The fatigue tests of composite samples were conducted in a load-controlled manner with a constant amplitude loading. In load-controlled fatigue tests, the maximum and minimum loads (and therefore maximum stress (σ_{max}) and minimum stress (σ_{max})) remain constant throughout the test. As damage develops due to fatigue, the strength and rigidity of the test specimen gradually decrease, leading to an increase in the amount of deformation over time. Fatigue tests were conducted at two different stress amplitudes (S) with constant stress ratio ($R = 0.1$). The stress amplitude (S) can calculated by (3.2). In this equation, σ_{max} and σ_{ult} represent the maximum stress and the ultimate strength of the composite material, respectively.

$$S = \frac{\sigma_{max}}{\sigma_{ult}} \tag{3.2}$$

In fatigue tests, the load was applied to the test specimen sinusoidally and consistently at a frequency of 5 Hz. The obtained raw data was then transformed into stress-cycle number curves and plotted on a graph. Simultaneous electrical resistance measurements were conducted to monitor the level of fatigue-related damage during fatigue tests. The electrical resistance change rates as percentage were determined at failure for two different stress amplitude (S). Five samples were tested for each amplitude ratio. Finally, reliability analysis of the electrical resistance change rate at the moment of damage was conducted using Weibull analysis. Consequently, reliability graphs were

obtained, allowing the determination of electrical resistance change rates that prevent fatigue damage at the desired reliability level. The stiffness loss ratio – cycle number ($\Delta E_{loss} - N$) curves and the resistance change ratio - cycle number ($\Delta R - N$) curves obtained through simultaneous resistance measurement were combined in a single graph. The stiffness loss ratio due to fatigue in each cycle (ΔE_{loss}) was determined by (3.3) and the electrical resistance change ratio (ΔR) was obtained using (3.4). In (3.3), E_0 represents the elastic modulus in the unloaded state, and E_i represents the stiffness after each cycle. In (3.4), R_i represents the resistance obtained after each cycle, while R_0 represents the initial resistance of the composite samples in the unloaded state.

$$\Delta E_{loss}\ (\%)_i = \frac{E_0 - E_i}{E_0} x100 \tag{3.3}$$

$$\Delta \mathrm{R}\ (\%) = \frac{R_i - R_0}{R_0} x100 \tag{3.4}$$

$$E_i = \frac{\sigma_{max} - \sigma_{min}}{\varepsilon_{max} - \varepsilon_{min}} \tag{3.5}$$

4. RESULTS AND DISCUSSION

4.1. Electrical Resistance Measurements of Unreinforced Nanocomposites

The purpose of the electrical resistance measurement of CNT filled epoxy composites was to determine the optimum dispersion parameters of ultrasonication method. Figure 4.1 compares the specific electrical resistance values of 0.2 wt% CNT-filled epoxy composites dispersed at varying power for 20 min as a list and column bar.

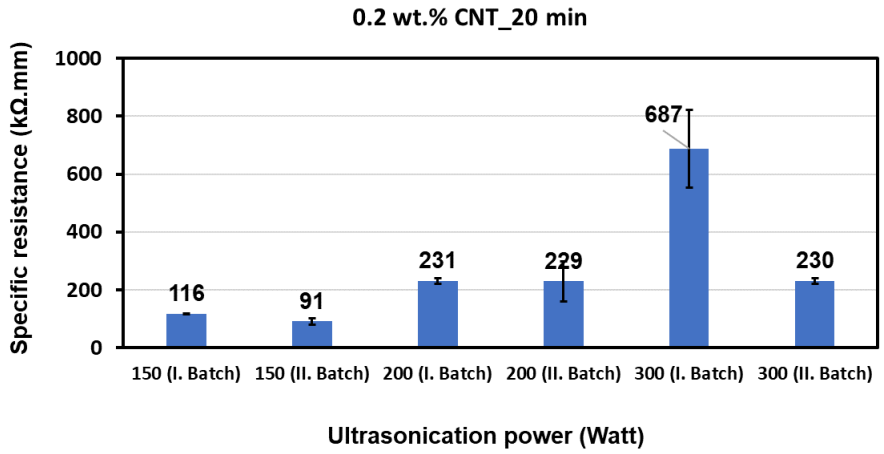

Figure 4.1. *The specific electrical resistance values of 0.2 wt% CNT-filled epoxy composites dispersed at varying power for 20 min.*

The results show that the lowest and highest resistance is seen at 150 W and 300 W, respectively. Since it is known that the better dispersion of CNTs in epoxy results in lower electrical resistivity (or higher conductivity) the ultrasonic dispersion at a greater power than 150 W is not efficient in terms of dispersion quality. Therefore, the effect of the dispersion time was investigated on the dispersion quality in terms of electrical resistivity at 150 W. Figure 4.2 compares the specific electrical resistance values of 0.2 wt% CNT-filled epoxy composites dispersed at 150 W power for varying dispersion time as a list and column bar. The results indicate that the lowest resistance is seen at 20 min of dispersion time. Based on these findings, the optimum dispersion parameters of nanoparticles in epoxy matrix was decided as 150 W for power and 20 min for dispersion time. It would be expected that the higher ultrasonication power and the dispersion time, the greater the electrical conductivity and consequently better dispersion quality. However, the electrical properties do not only depend on the dispersion level but also the aspect ratio of the filler material. Therefore, these results in this study might be due to reduction in the aspect ratio of CNTs as a result of aggressive dispersion process of

ultrasonication at higher ultrasonication power and longer dispersion time as discussed in the literature (Foundation et al., 1996).

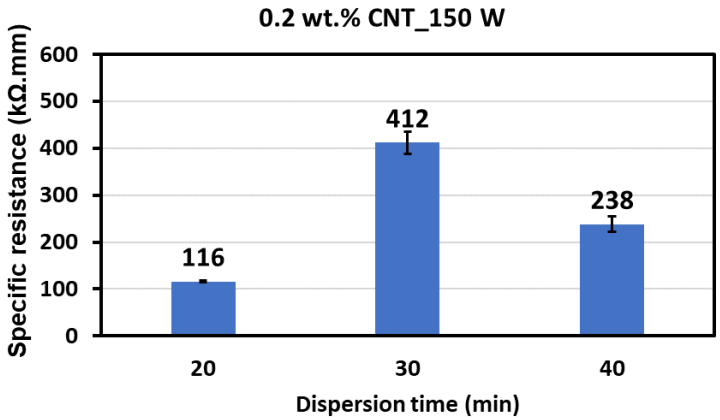

Figure 4.2. *The specific electrical resistance values of 0.2 wt% CNT-filled epoxy composites dispersed at 150 W for varying dispersion time*

4.2. Electrical Resistance Measurements of Glass Fiber Reinforced Nanocomposites

Figure 4.3 shows the effect of CNT concentration on the electrical resistance of glass fiber-reinforced composite. As expected, an increase in the CNT concentration results in a decrease in the electrical resistance of the composite samples. In other words, as the CNT concentration increases, the electrical conductivity of the composite samples increases. The resistance measurement capacity of the digital multimeter used in the thesis is a maximum of 2 GΩ. In measurements of samples filled with 0.1% CNT, no measurement was obtained from the device, because the electrical resistance change value at this ratio is greater than 2 GΩ. At the 0.2% CNT content, there is a very sharp increase in conductivity.

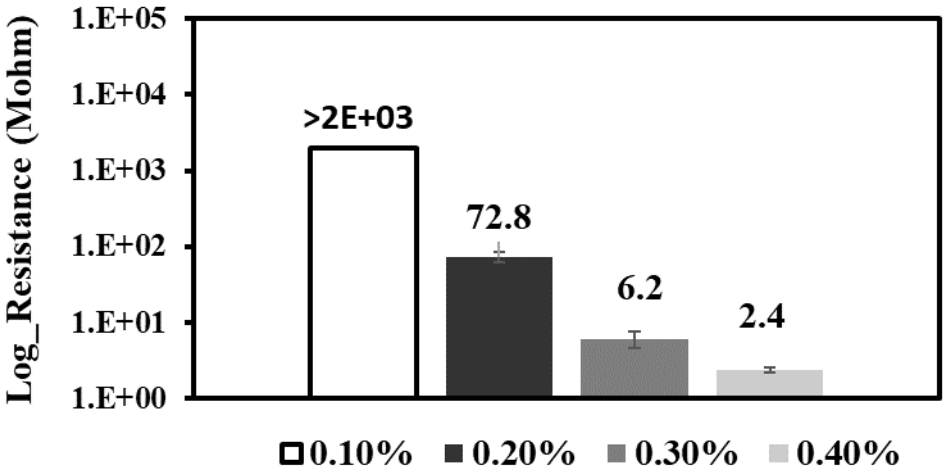

Figure 4.3. *The effect of CNT concentration on the electrical properties of glass fiber reinforced epoxy nanocomposites*

4.3. Static Tensile Tests of Glass Reinforced Nanocomposites

Figure 4.4 provides a comparative representation of the average tensile strength and elastic modulus of glass fiber reinforced nanocomposites for varying MWCNT concentrations. The results indicate an enhancement in the mechanical properties of the glass fiber-reinforced composite due to MWCNT reinforcement. The increase in tensile strength for 0.1%, 0.2%, 0.3%, and 0.4% MWCNT filled composite samples is respectively 22%, 18%, 31%, and 13%, while the increase in elastic modulus is 43%, 33%, 47%, and 28% in the same order. These findings clearly demonstrate the reinforcing properties of GNPs.

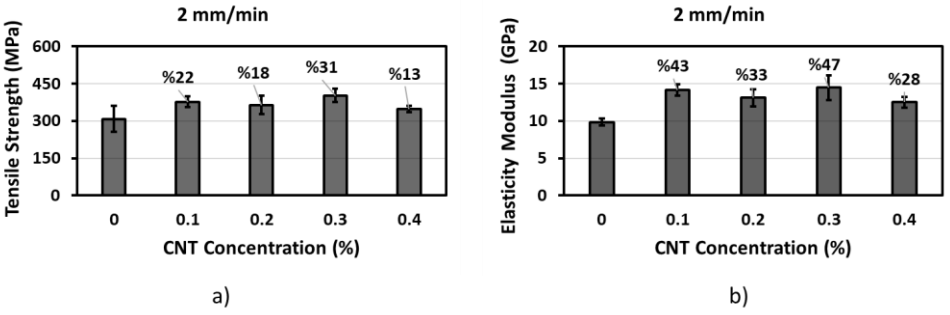

Figure 4.4. *The effect of CNT concentration on the mechanical properties of glass fiber reinforced epoxy nanocomposites*

4.4. Fatigue Tests

The composites should be electrically conductive for reliable damage sensing during fatigue testing. Therefore, samples filled with 0.2%, 0.3%, and 0.4% CNT

concentration could be used to detect the damage in composite materials during fatigue tests through simultaneous electrical resistance change method. The electrical conductivity at the CNT concentrations higher than 0.2 % is desirable for reliable sensing due to the better CNT network density within composite. In addition, highest improvement in the mechanical properties was observed when 0.3 % CNT concentration was employed in the composites. Therefore, 0.3 % wt. CNT filled composites were used in fatigue testing for in-situ health monitoring process.

Since the average ultimate strength of 0.3 % wt. CNT filled composites was obtained as 400 MPa, fatigue test procedure was conducted at two stress amplitude (S) as summarized in Table 4.1.

Table 4. 1. *Fatigue test procedure*

Static Tensile Strength (MPa)	Maximum Stress (MPa)	Minimum Stress (MPa)	Stress Amplitude (MPa)	Stress Ratio
400	240	24	0.6	0.1
	200	20	0.5	

Figures 4.5 and 4.6 show the stress-cycle number diagrams obtained from fatigue tests conducted at stress amplitudes of S=0.6 and S=0.5, respectively. It is observed that both maximum and minimum stresses remain constant during the entire testing process for all tests as expected in force-controlled fatigue tests.

Figures 4.7 and 4.8 show the displacement-cycle number diagrams obtained from fatigue tests conducted at stress amplitudes of S=0.6 and S=0.5, respectively. It is seen that samples exhibit greater displacement with increasing cycle number in all tests due to the damage accumulation resulting in rigidity lost in the composite specimens.

Figures 4.9 and 4.10 illustrate stress-strain curves obtained from fatigue tests conducted at strain ratios of S=0.6 and S=0.5, respectively. Notably, the graphs reveal a progressive reduction in the slopes of the stress-strain curves after each cycle, attributed to a decline in rigidity. This phenomenon is indication of a loss in stiffness, due to the fatigue damage.

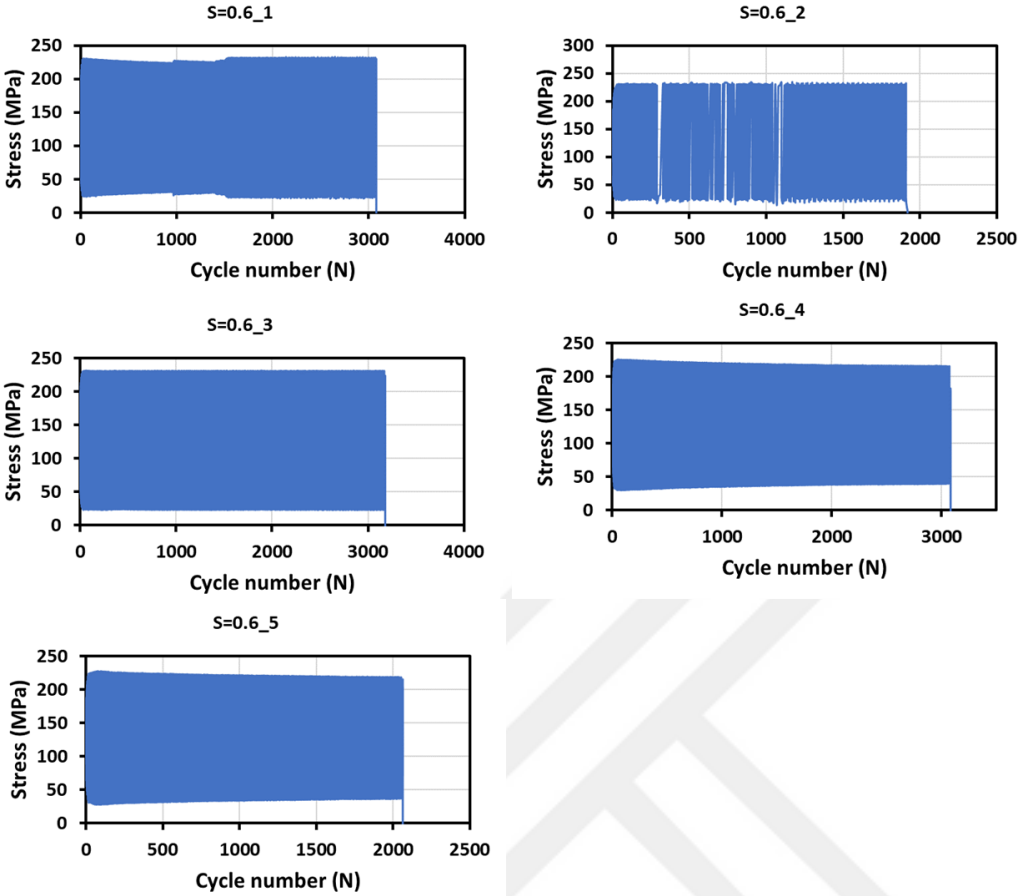

Figure 4.5. *Stress–cycle number curves obtained from fatigue tests conducted at an amplitude ratio of S=0.6.*

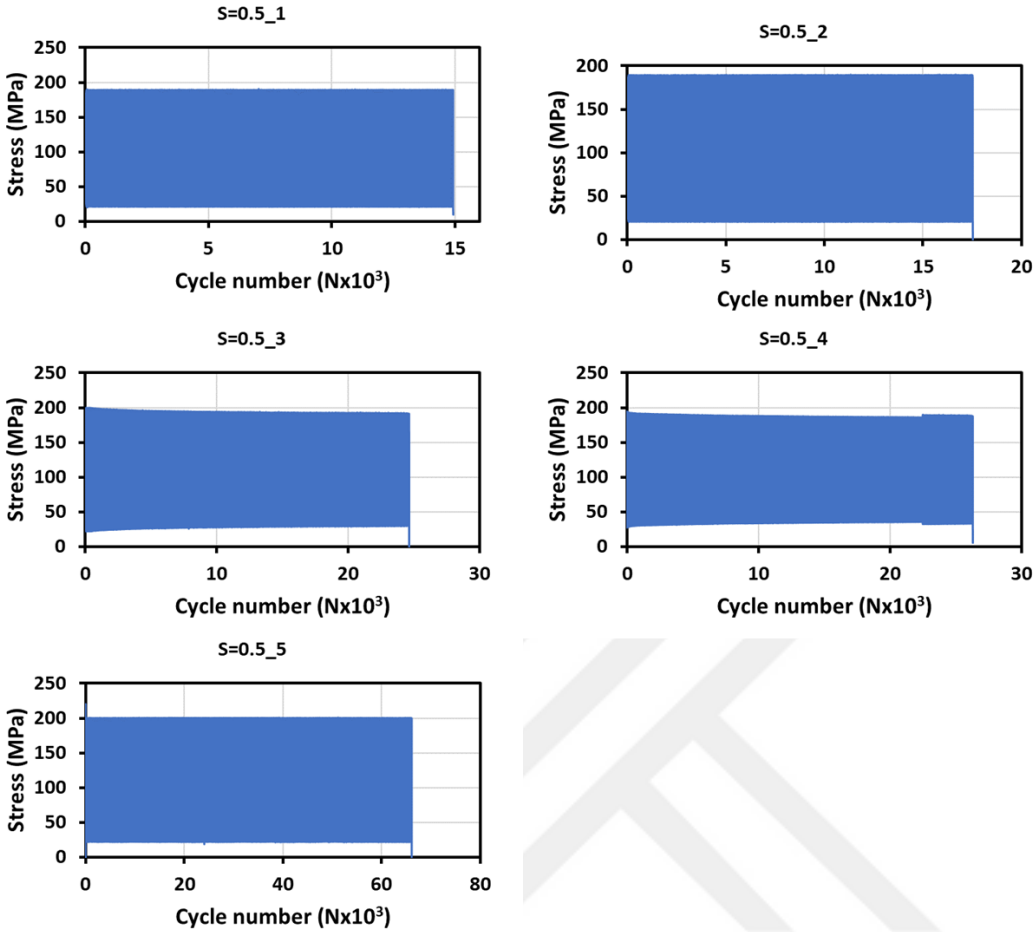

Figure 4.6. *Stress–cycle number curves obtained from fatigue tests conducted at an amplitude ratio of S=0.5.*

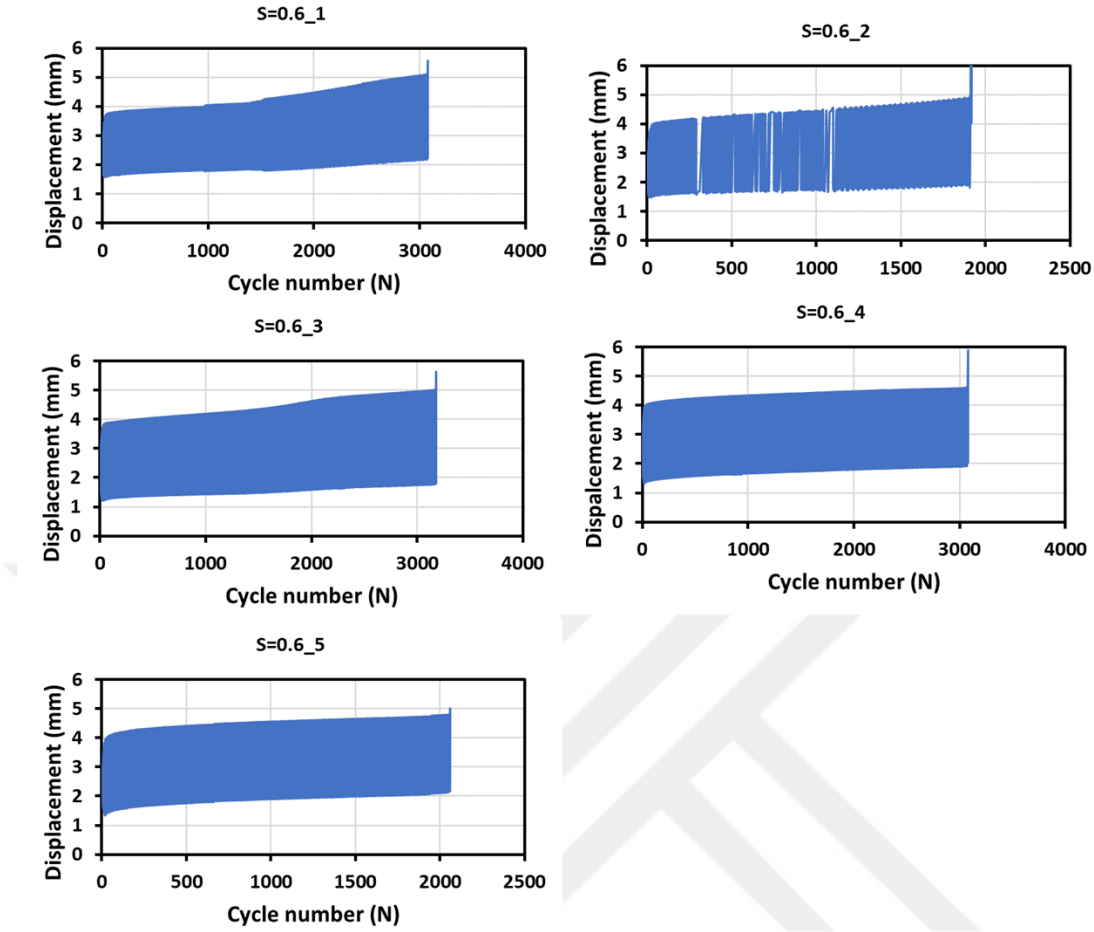

Figure 4.7. *Displacement–cycle number curves obtained from fatigue tests conducted at an amplitude ratio of S=0.6.*

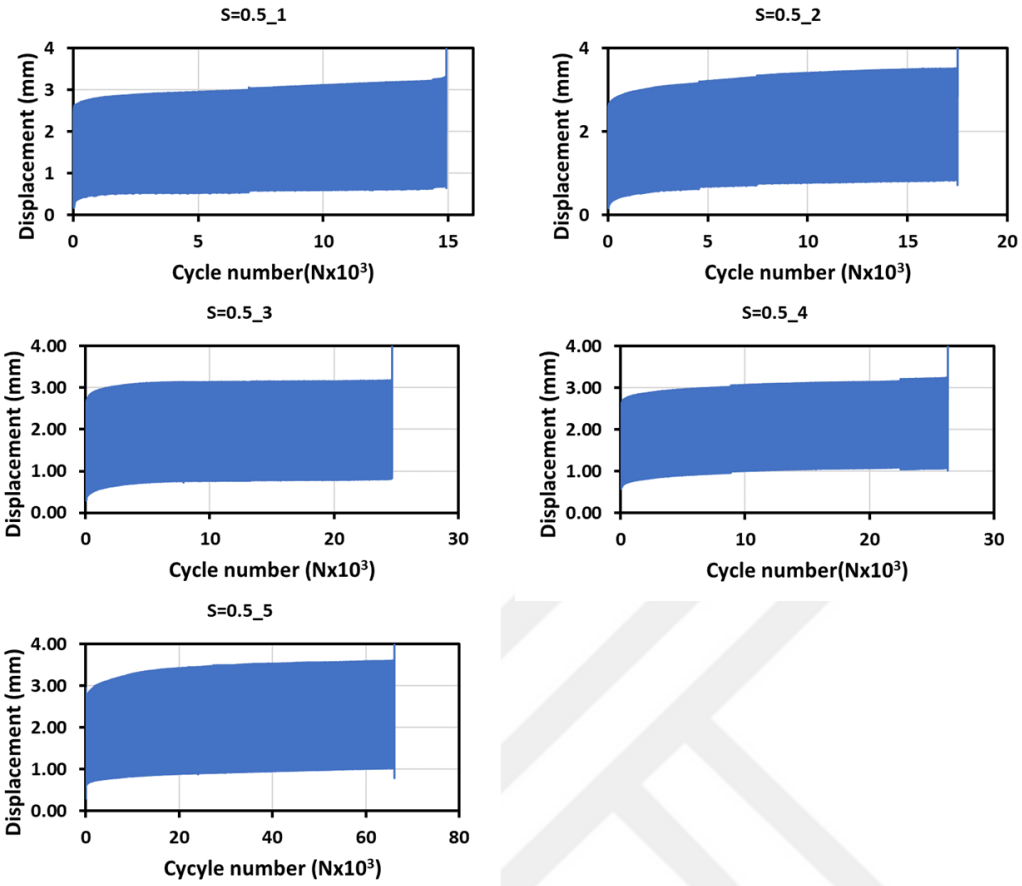

Figure 4.8. *Displacement–cycle number curves obtained from fatigue tests conducted at an amplitude ratio of S=0.5.*

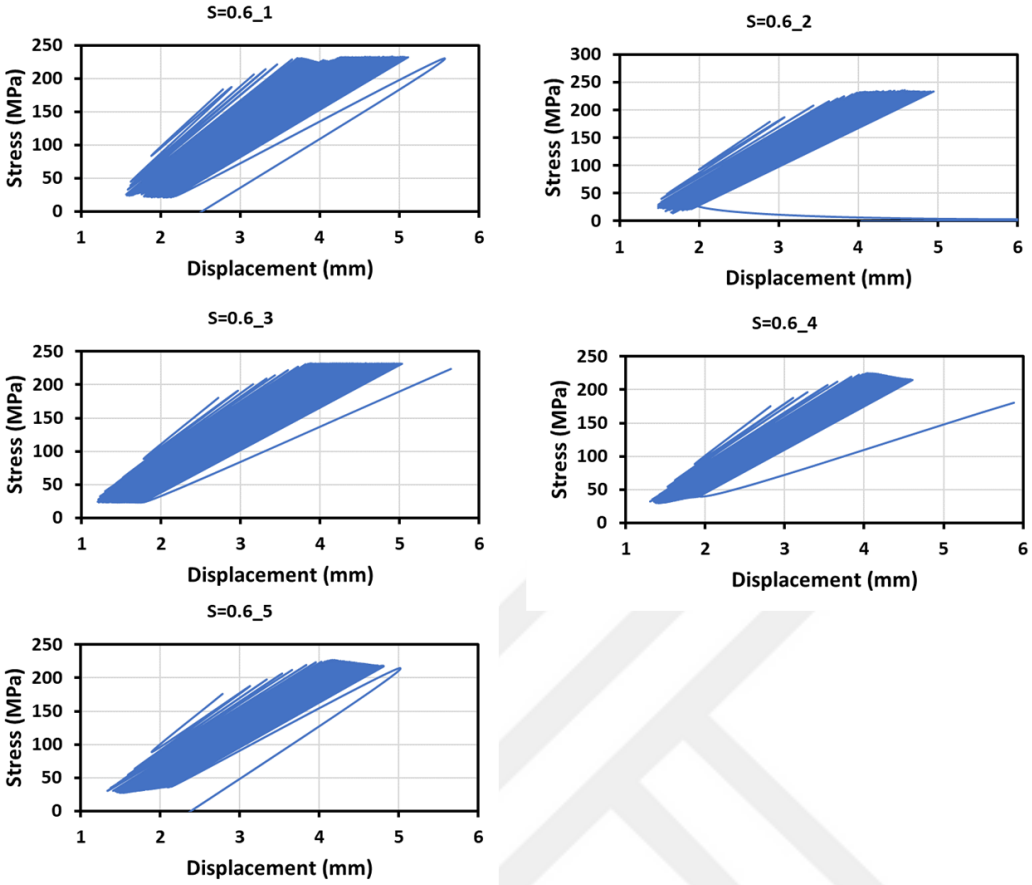

Figure 4.9. *Stress–displacement curves obtained from fatigue tests conducted at an amplitude ratio of S=0.6*

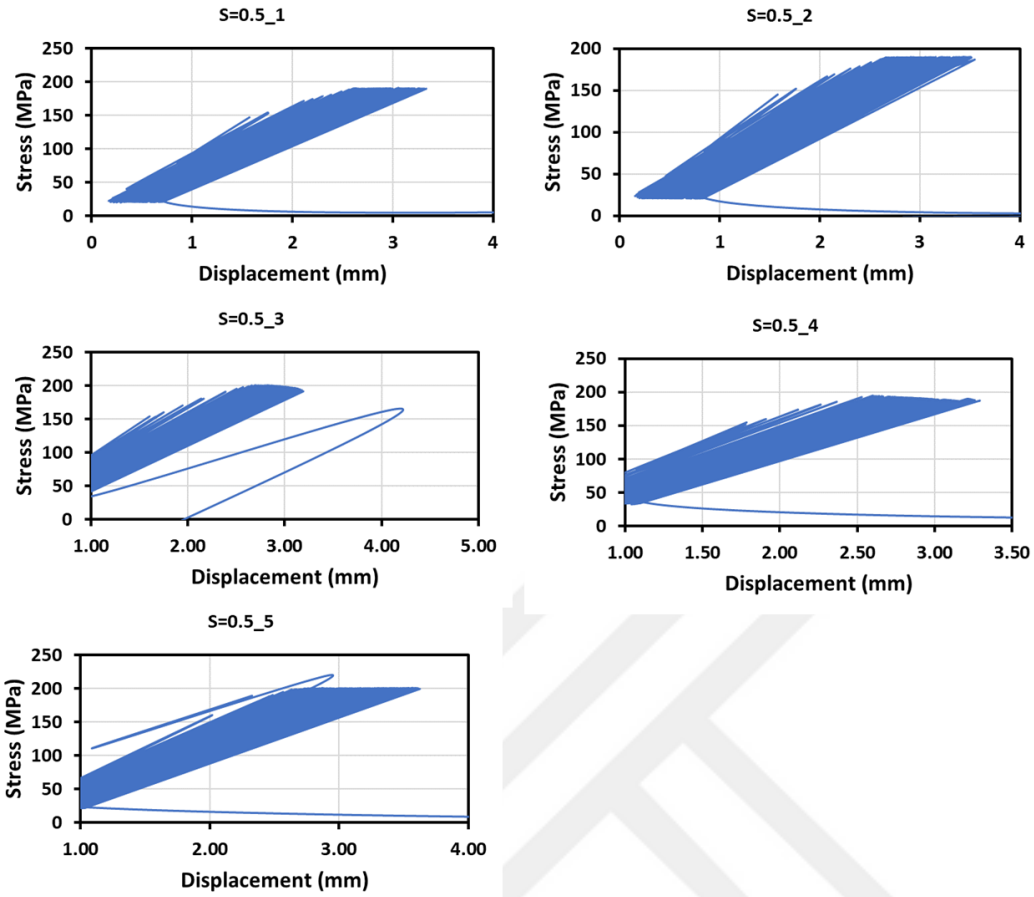

Figure 4.10. *Stress–displacement curves obtained from fatigue tests conducted at an amplitude ratio of S=0.5*

4.5. Damage Sensing by Electrical Resistance Change Method

Electrical resistance change of specimens were simultaneously measured during fatigue tests to monitor fatigue damage accumulation inside the composites. Figure 4.11 and 4.12 illustrates the relationships among stiffness loss, cycle number, and resistance change obtained from fatigue tests at stress amplitudes of S=0.6 and S=0.5, respectively. The graphs reveal that fatigue – induced damage leads to reduction in stiffness loss and consequently to increase in electrical resistance. The increase in the electrical resistance is mainly due to the fact that damages such as matrix cracks and fiber breakages reduce the electrically conductive CNT networks within composite.

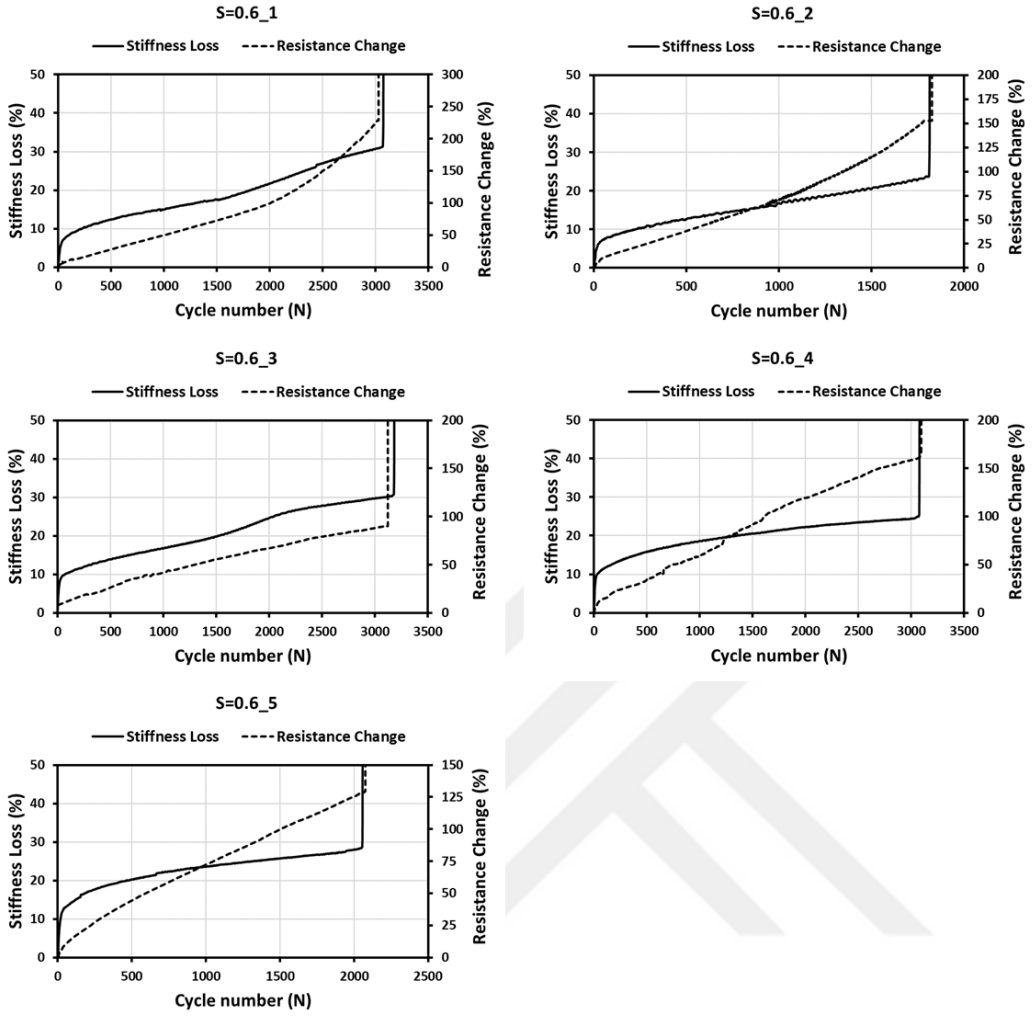

Figure 4.11. *Stiffness loss – Resistance change – Cycle number curves obtained from fatigue tests at S=0.6.*

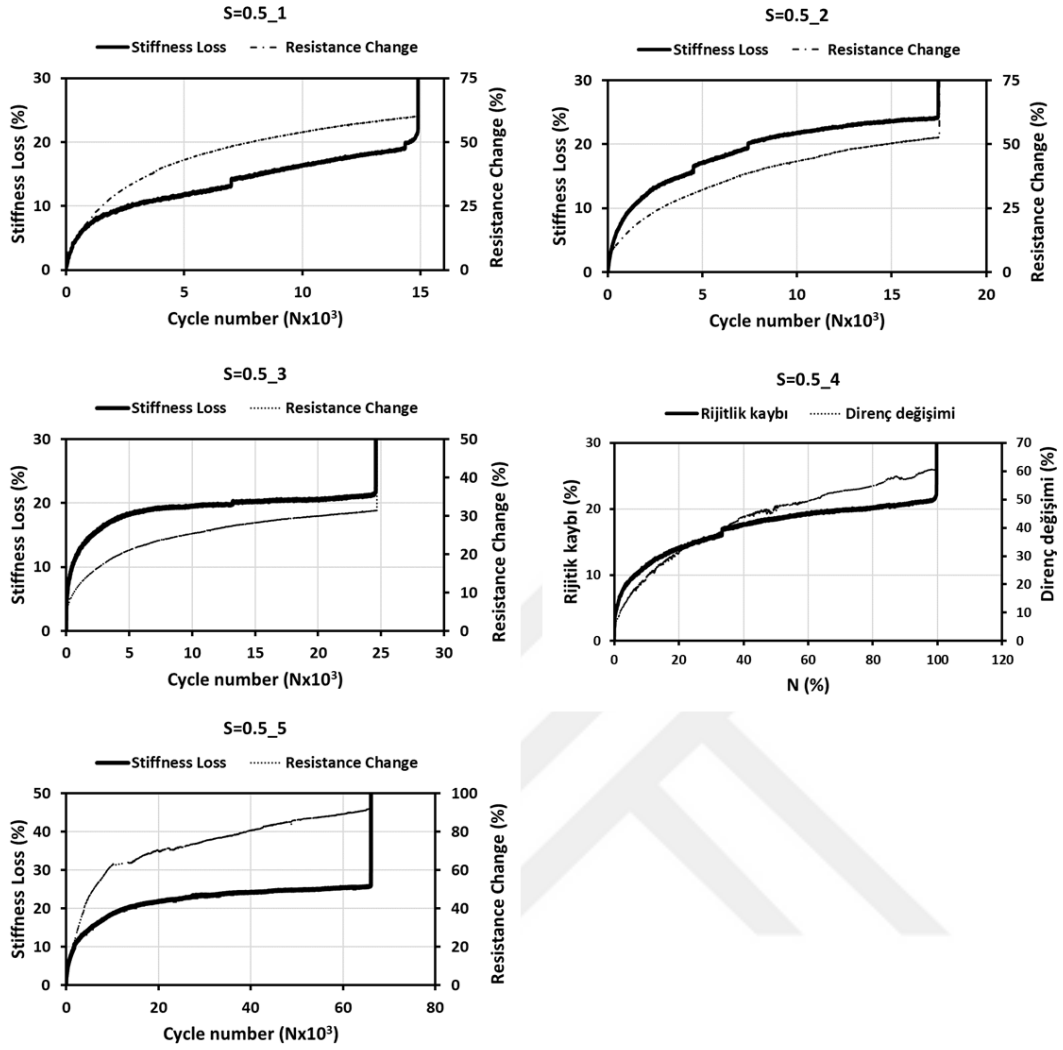

Figure 4.12. *Stiffness loss – Resistance change – Cycle number curves obtained from fatigue tests at S=0.5*

Figures 4.13 and 4.14 show the variation of resistance change and stiffness loss with respect to cycle number as well as fatigue life for S=0.6 and S=0.5, respectively. In general, the specimens tested at the same stress amplitude exhibit almost same type of resistance change characteristic and stiffness loss behavior which is a good indication for the reliable sensing behavior of composites.

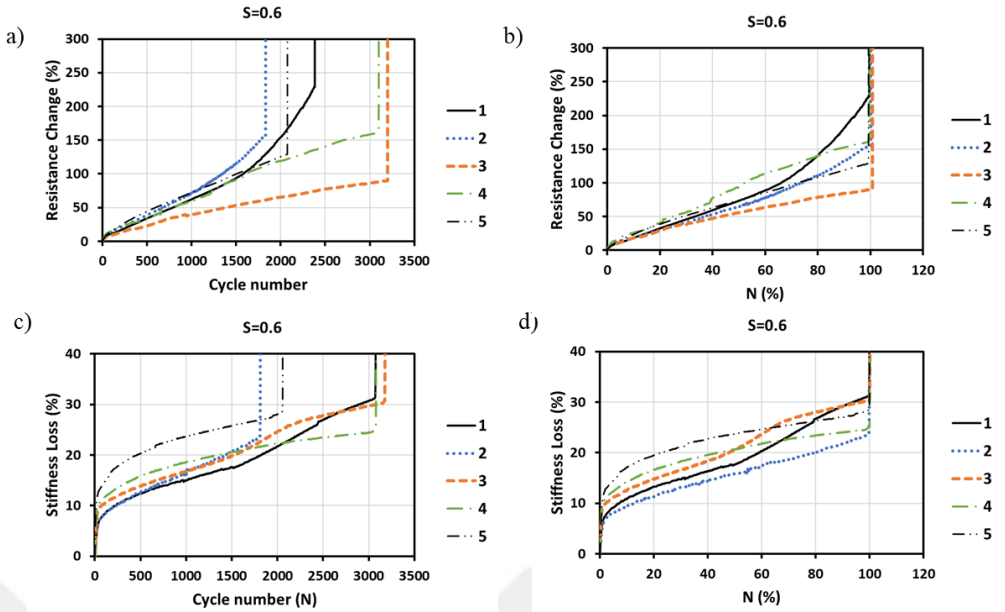

Figure 4.13. *a) Resistance change – cycle number, b) Resistance change – fatigue life, c) Stiffness loss – cycle number, and d) Stiffness loss – fatigue life curves for S=0.6*

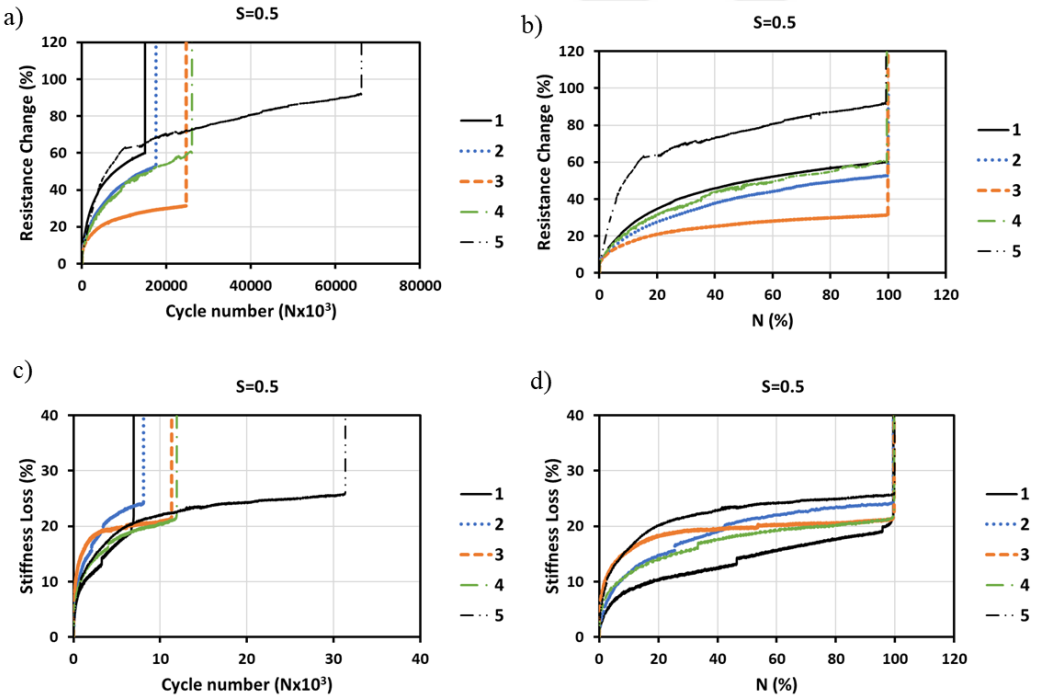

Figure 4.14. *a) Resistance change – cycle number, b) Resistance change – fatigue life, c) Stiffness loss – cycle number, and d) Stiffness loss – fatigue life curves for S=0.5*

Figures 4.15 and 4.16 compare the average values of resistance change, stiffness loss, and cycle number corresponding to 100% (at failure), 80%, 60%, and 40% fatigue life for stress amplitudes of S=0.6 and S=0.5, respectively. As expected, it is observed that as the stress amplitude decreases, the fatigue life increases. The average cycle

numbers at the failure were found as 2,638, and 30,000 for S=0.6 and S=0.5, respectively. The average stiffness loss values at the failure for S=0.6 and S=0.5 were observed to be 28% and 25%, respectively. The stiffness loss during fatigue test might be affected by some parameters such as material type, stress amplitude, and the testing conditions. It is noted that stiffness loss at S=0.6 is greater than that of at S=0.5. This result indicates that the higher stress amplitudes caused more significant material damage and faster degradation in stiffness. However, the difference in the stiffness loss between higher stress amplitude (S=0.6) and lower stress amplitude (S=0.5) does not seem significant. The average percentage resistance change values at the failure for S=0.6 and S=0.5 were observed to be 153% and 59%, respectively. This result reveals that the electrical resistance change values also exhibit dependence on the stress amplitude. Since stiffness loss is associated with the damage mechanisms such as matrix crack formation, fiber breakage, and delamination, these mechanisms also deteriorates electrically conductive CNT networks resulting in increase in the electrical resistance. It is also interesting to note that increase in the stiffness loss during fatigue test is significantly lower than the increase in the electrical resistance change. For example, the difference in the stiffness loss between N=40% and N=100% occurred as 10% whereas this difference in the electrical resistance change was observed as 93% for S=0.6. The same trend can be observed in the case of S=0.5.

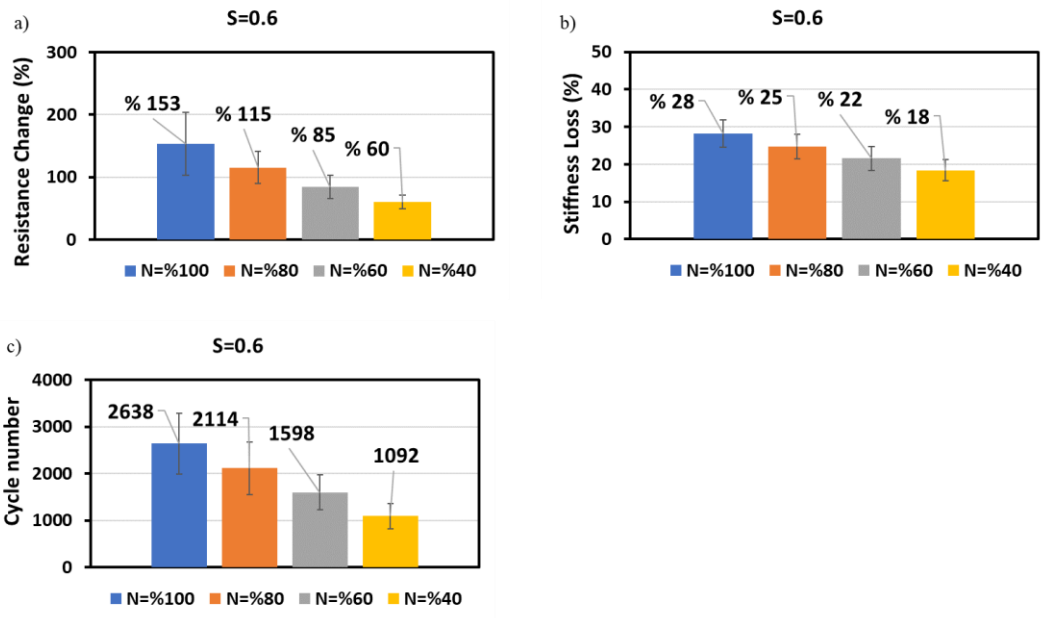

Figure 4.15. *Average values of a) resistance change, b) stiffness loss, and c) cycle number obtained from the fatigue tests at S=0.6*

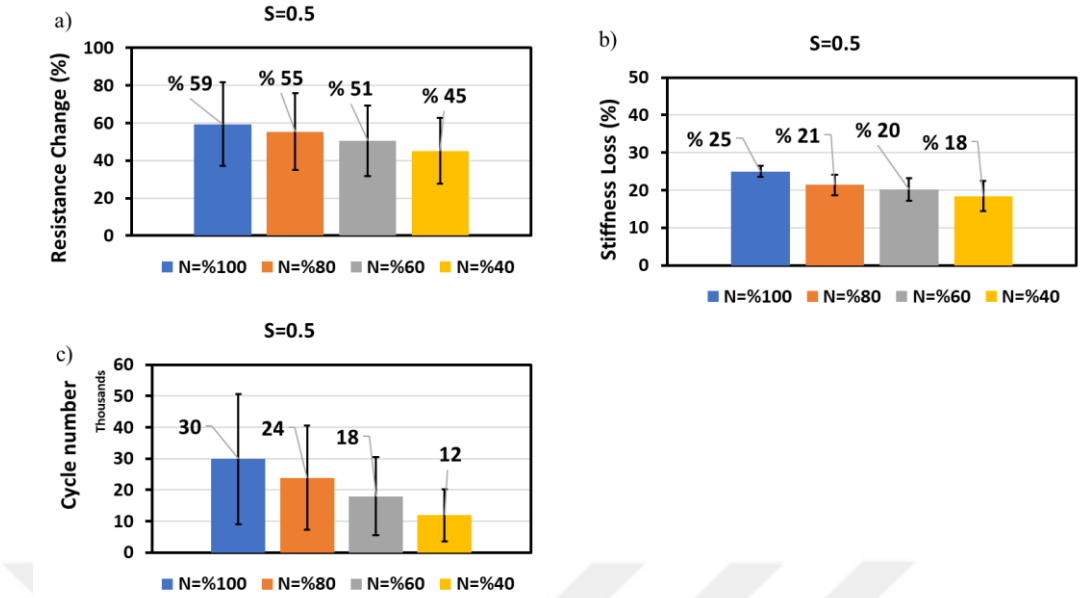

Figure 4.16. *Average values of a) resistance change, b) stiffness loss, and c) cycle number obtained from the fatigue tests at S=0.5*

4.6. Weibull Analysis

4.6.1. Weibull distribution analysis for cycle number

Table 4.2- 4.5 shows the cycle numbers in ascending order along with the corresponding parameters of Weibull analysis for S=0.6 at the 100%, 80%, 60%, and 40% fatigue life, respectively. Similarly, Table 4.6 - 4.9 shows the Weibull distribution parameters for S=0.5.

Table 4.2. *Cycle numbers in ascending order along with the corresponding parameters of Weibull analysis for N = 100% and S = 0.6*

S=0.6 (N=%100)							
N	**Rank**	**Median Rank (MR)**	**ln(N)**	**ln(ln(1/(1-MR)))**	**Lineer Equation**	**α**	**β**
1810	1	0.13	7.50	-1.97	y = 3.6152x - 28.873 R² = 0.8556	2941.152	3.6152
2055	2	0.31	7.63	-0.97			
3074	3	0.50	8.03	-0.37			
3075	4	0.69	8.03	0.14			
3175	5	0.87	8.06	0.71			

Table 4.3. *Cycle numbers in ascending order along with the corresponding parameters of Weibull analysis for N = 80% and S = 0.6*

S=0.6 (N=%80)							
N	**Rank**	**Median Rank (MR)**	**ln(N)**	**ln(ln(1/(1-MR)))**	**Lineer Equation**	**α**	**β**
1500	1	0.13	7.31	-1.97	y = 3.7378x - 29.002 R² = 0.9414	2342.818	3.7378
1640	2	0.31	7.40	-0.97			
2095	3	0.50	7.65	-0.37			
2535	4	0.69	7.84	0.14			
2800	5	0.87	7.94	0.71			

Table 4.4. *Cycle numbers in ascending order along with the corresponding parameters of Weibull analysis for N = 60% and S = 0.6*

S=0.6 (N=%60)							
N	**Rank**	**Median Rank (MR)**	**ln(N)**	**ln(ln(1/(1-MR)))**	**Lineer Equation**	**α**	**β**
1070	1	0.13	6.98	-1.97	y = 4.007x - 29.952 R² = 0.9487	1763.259	4.007
1365	2	0.31	7.22	-0.97			
1775	3	0.50	7.48	-0.37			
1795	4	0.69	7.49	0.14			
1985	5	0.87	7.59	0.71			

Table 4.5. *Cycle numbers in ascending order along with the corresponding parameters of Weibull analysis for N = 40% and S = 0.6*

S=0.6 (N=%40)							
N	**Rank**	**Median Rank (MR)**	**ln(N)**	**ln(ln(1/(1-MR)))**	**Lineer Equation**	**α**	**β**
800	1	0.13	6.68	-1.97	y = 3.7642x - 26.725 R² = 0.883	1211.703	3.7642
820	2	0.31	6.71	-0.97			
1180	3	0.50	7.07	-0.37			
1230	4	0.69	7.11	0.14			
1430	5	0.87	7.27	0.71			

Table 4.6. *Cycle numbers in ascending order along with the corresponding parameters of Weibull analysis for N = 100% and S = 0.5*

S=0.5 (N=%100)							
N	**Rank**	**Median Rank (MR)**	**ln(N)**	**ln(ln(1/(1-MR)))**	**Lineer Equation**	**α**	**β**
14940	1	0.13	9.61	-1.97	y = 1.5934x - 16.667 R² = 0.7888	34892.34	1.5934
17500	2	0.31	9.77	-0.97			
24600	3	0.50	10.11	-0.37			
26000	4	0.69	10.17	0.14			
66140	5	0.87	11.10	0.71			

Table 4.7. *Cycle numbers in ascending order along with the corresponding parameters of Weibull analysis for N = 80% and S = 0.5*

S=0.5 (N=%80)							
N	**Rank**	**Median Rank (MR)**	**ln(N)**	**ln(ln(1/(1-MR)))**	**Lineer Equation**	**α**	**β**
11952	1	0.13	9.39	-1.97	y = 1.5934x - 16.311 R² = 0.7888	27906.11	1.5934
14000	2	0.31	9.55	-0.97			
19680	3	0.50	9.89	-0.37			
20800	4	0.69	9.94	0.14			
52912	5	0.87	10.88	0.71			

Table 4.8. *Cycle numbers in ascending order along with the corresponding parameters of Weibull analysis for N = 60% and S = 0.5*

S=0.5 (N=%60)							
N	**Rank**	**Median Rank (MR)**	**ln(N)**	**ln(ln(1/(1-MR)))**	**Lineer Equation**	**α**	**β**
8964	1	0.13	9.10	-1.97	y = 1.5934x - 15.853 R² = 0.7888	20934.74	1.5934
10500	2	0.31	9.26	-0.97			
14760	3	0.50	9.60	-0.37			
15600	4	0.69	9.66	0.14			
39684	5	0.87	10.59	0.71			

Table 4.9. *Cycle numbers in ascending order along with the corresponding parameters of Weibull analysis for N = 40% and S = 0.5*

S=0.5 (N=%40)							
N	**Rank**	**Median Rank (MR)**	**ln(N)**	**ln(ln(1/(1-MR)))**	**Lineer Equation**	**α**	**β**
5976	1	0.13	8.70	-1.97	y = 1.5934x - 15.207 R² = 0.7888	13957.09	1.5934
7000	2	0.31	8.85	-0.97			
9840	3	0.50	9.19	-0.37			
10400	4	0.69	9.25	0.14			
26456	5	0.87	10.18	0.71			

Figure 4.17 shows the comparative curves drawn on the x-axis with ln (fatigue life (N)) values and on the y-axis with $\ln(\ln(1/(1-MR)))$, for each fatigue life. Linear regression was applied to each fatigue life on the graph. The equations obtained from the linear regression results provided the values of α (characteristic life) and β (shape parameter). Subsequently, using the reliability function (2.4 or 2.7), reliability graphs based on the number of cycles were obtained (Figure 4.18).

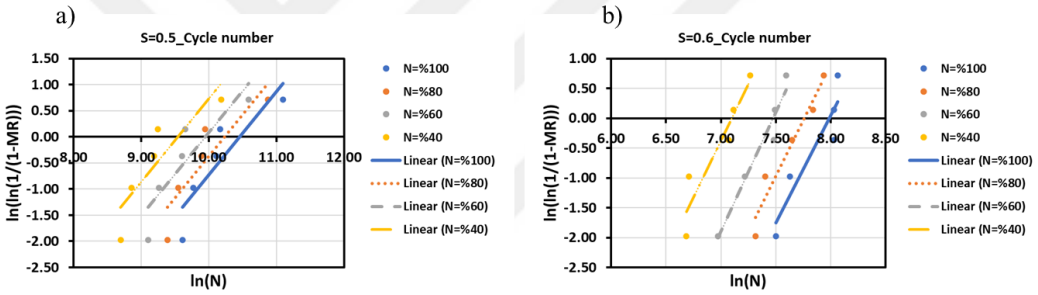

Figure 4.17. *Weibull distribution curves for cycle number at the stress amplitudes of a) S=0.5 and b) S=0.6.*

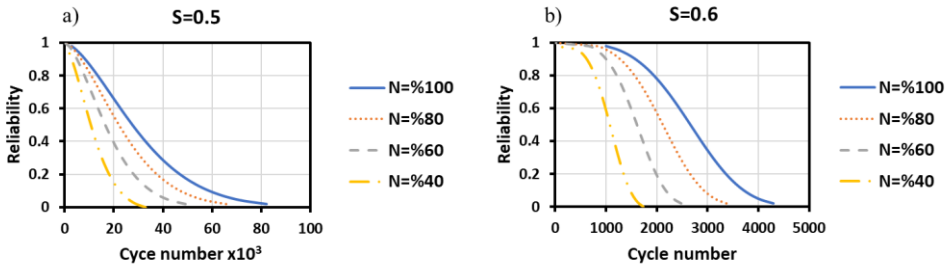

Figure 4.18. *Reliability curves for cycle number at the stress amplitudes of a) S=0.5 and b) S=0.6.*

4.6.2. Weibull distribution analysis for electrical resistance change

Tables 4.10- 4.13 show the electrical resistance change values in ascending order along with the corresponding parameters of Weibull analysis for S=0.6 at the 100%, 80%, 60%, and 40% fatigue life, respectively. Similarly, Tables 4.14 - 4.17 show the Weibull distribution parameters of electrical resistance change values for S=0.5.

Table 4.10. *Electrical resistance changes ΔR (%) in ascending order along with the corresponding parameters of Weibull analysis for N = 100% and S = 0.6*

S=0.6 (N=%100)							
ΔR (%)	**Rank**	**Median Rank (MR)**	**ln(ΔR)**	**ln(ln(1/(1-MR)))**	**Lineer Equation**	**α**	**β**
90	1	0.13	4.50	-1.97	y = 3.0107x - 15.5 R² = 0.9724	172.13936	3.0107
130	2	0.31	4.87	-0.97			
153	3	0.50	5.03	-0.37			
164	4	0.69	5.10	0.14			
228	5	0.87	5.43	0.71			

Table 4.11. *Electrical resistance changes ΔR (%) in ascending order along with the corresponding parameters of Weibull analysis for N = 80% and S = 0.6*

S=0.6 (N=%80)							
ΔR (%)	**Rank**	**Median Rank (MR)**	**ln(ΔR)**	**ln(ln(1/(1-MR)))**	**Lineer Equation**	**α**	**β**
79	1	0.13	4.37	-1.97	y = 4.2891x - 20.767 R² = 0.9369	126.6982538	4.2891
108	2	0.31	4.68	-0.97			
111	3	0.50	4.71	-0.37			
139	4	0.69	4.93	0.14			
140	5	0.87	4.94	0.71			

Table 4.12. *Electrical resistance changes ΔR (%) in ascending order along with the corresponding parameters of Weibull analysis for N = 60% and S = 0.6*

S=0.6 (N=%60)							
ΔR (%)	**Rank**	**Median Rank (MR)**	**ln(ΔR)**	**ln(ln(1/(1-MR)))**	**Lineer Equation**	**α**	**β**
64	1	0.13	4.16	-1.97	y = 4.7084x - 21.378 R² = 0.9282	93.72789854	4.7084
78	2	0.31	4.36	-0.97			
85	3	0.50	4.44	-0.37			
88	4	0.69	4.48	0.14			
115	5	0.87	4.74	0.71			

Table 4.13. *Electrical resistance changes ΔR (%) in ascending order along with the corresponding parameters of Weibull analysis for N = 40% and S = 0.6*

S=0.6 (N=%40)							
ΔR (%)	**Rank**	**Median Rank (MR)**	**ln(ΔR)**	**ln(ln(1/(1-MR)))**	**Lineer Equation**	**α**	**β**
47	1	0.13	3.85	-1.97	y = 5.7633x - 23.957 R² = 0.9637	63.86809095	5.7633
53	2	0.31	3.97	-0.97			
59	3	0.50	4.08	-0.37			
63	4	0.69	4.14	0.14			
75	5	0.87	4.32	0.71			

Table 4.14. *Electrical resistance changes ΔR (%) in ascending order along with the corresponding parameters of Weibull analysis for N = 100% and S = 0.5*

S=0.5 (N=%100)							
ΔR (%)	**Rank**	**Median Rank (MR)**	**ln(ΔR)**	**ln(ln(1/(1-MR)))**	**Lineer Equation**	**α**	**β**
31	1	0.13	3.43	-1.97	y = 2.5303x - 10.676 R² = 0.9213	67.98333	2.5303
53	2	0.31	3.97	-0.97			
60	3	0.50	4.09	-0.37			
60	4	0.69	4.09	0.14			
93	5	0.87	4.53	0.71			

Table 4.15. *Electrical resistance changes ΔR (%) in ascending order along with the corresponding parameters of Weibull analysis for N = 80% and S = 0.5*

S=0.5 (N=%80)							
ΔR (%)	**Rank**	**Median Rank (MR)**	**ln(ΔR)**	**ln(ln(1/(1-MR)))**	**Lineer Equation**	**α**	**β**
30	1	0.13	3.40	-1.97	y = 2.6221x - 10.87 R² = 0.9251	63.15122	2.6221
49	2	0.31	3.89	-0.97			
55	3	0.50	4.01	-0.37			
56	4	0.69	4.03	0.14			
87	5	0.87	4.47	0.71			

Table 4.16. *Electrical resistance changes* $\Delta \boldsymbol{R}$ (%) *in ascending order along with the corresponding parameters of Weibull analysis for N = 60% and S = 0.5*

S=0.5 (N=%60)							
ΔR (%)	**Rank**	**Median Rank (MR)**	**ln(ΔR)**	**ln(ln(1/(1-MR)))**	**Lineer Equation**	**α**	**β**
28	1	0.13	3.33	-1.97	y = 2.67x - 10.819 R² = 0.9368	57.51581	2.67
44	2	0.31	3.78	-0.97			
49	3	0.50	3.89	-0.37			
52	4	0.69	3.95	0.14			
80	5	0.87	4.38	0.71			

Table 4.17. *Electrical resistance changes* $\Delta \boldsymbol{R}$ (%) *in ascending order along with the corresponding parameters of Weibull analysis for N = 40% and S = 0..*

S=0.5 (N=%40)							
ΔR (%)	**Rank**	**Median Rank (MR)**	**ln(ΔR)**	**ln(ln(1/(1-MR)))**	**Lineer Equation**	**α**	**β**
25	1	0.13	3.22	-1.97	y = 2.605x - 10.265 R² = 0.9365	51.44427	2.605
38	2	0.31	3.64	-0.97			
44	3	0.50	3.78	-0.37			
46	4	0.69	3.83	0.14			
73	5	0.87	4.29	0.71			

Figure 4.19 shows the comparative curves drawn on the x-axis with ln (resistance change (ΔR)) values and on the y-axis with $\ln(\ln(1/(1-MR)))$, for each fatigue life. Linear regression was applied to each fatigue life on the graph. The equations obtained from the linear regression results provided the values of α (characteristic life) and β (shape parameter). Subsequently, using the reliability function (2.4 or 2.7), reliability graphs based on the electrical resistance change values were obtained (Figure 4.20).

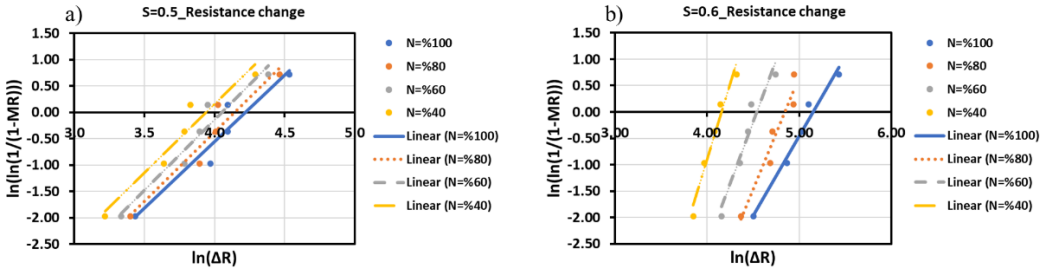

Figure 4.19. *Weibull distribution curves for resistance change at the stress amplitudes of a) S=0.5 and b) S=0.6.*

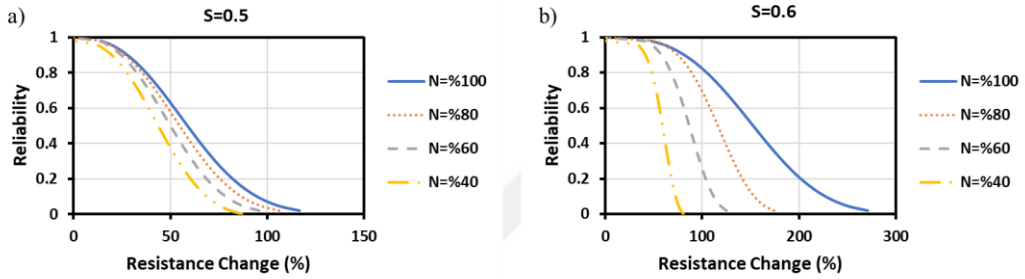

Figure 4.20. *Reliability curves for resistance change at the stress amplitudes of a) S=0.5 and b) S=0.6.*

4.7. Weibull Reliability for Cycle Number

Tables 4.18 and 4.19 show 95%, 80%, and 50% Weibull Reliability values of electrical resistance change and cycle number corresponding to various fatigue life for S=0.6 and S=0.5, respectively. Figure 4.21 provides a graphical comparison of the cycle number values extracted from Tables 4.18 and 4.19 to better illustrate the effect of the reliability analysis. In addition, Figure 4.22 compares the cycle number values to emphasize the effect of the stress amplitude on the cycle number. The average cycle numbers at the failure is almost identical with the values obtained at 50%Weibull reliability as expected. For the stress amplitudes of S=0.6 and S=0.5 at 100% fatigue life, the cycle numbers with 95% reliability were observed as 1360 and 6085, respectively. Figure 4.23 displays graphs of reliability-cycle number curves comparatively for two different stress amplitudes. It is seen that the cycle number of S=0.5 is greater than that of S=0.6 at all reliability and fatigue life.

Table 4.18. *95%, 80%, and 50% Weibull Reliability values of electrical resistance change and cycle number corresponding to various fatigue lifes for S=0.6*

S=0.6								
Fatigue Life	Average values (At failure)		Weibull Reliability					
			95%		80%		50%	
N (%)	*ΔR (%)*	*N*	*ΔR (%)*	*N*	*ΔR (%)*	*N*	*ΔR (%)*	*N*
100	153	2638	64	1360	104	1940	152	2657
80	115	2114	63	1110	89	1568	116	2123
60	85	1598	49	880	68	1212	86	1609
40	60	1092	37	570	49	813	60	1099

Table 4.19. *95%, 80%, and 50% Weibull Reliability values of electrical resistance change and cycle number corresponding to various fatigue lifes for S=0.5*

S=0.5								
Yorulma Ömrü	Hasar anı (Ortalama)		Weibull Reliability					
			95%		80%		50%	
N (%)	*ΔR (%)*	*N*	*ΔR (%)*	*N*	*ΔR (%)*	*N*	*ΔR (%)*	*N*
100	59	29836	23	6085	38	13611	59	27722
80	55	23869	22	4867	36	10866	55	22171
60	51	17902	20	3651	33	8166	50	16633
40	45	11934	18	2434	29	5444	45	11089

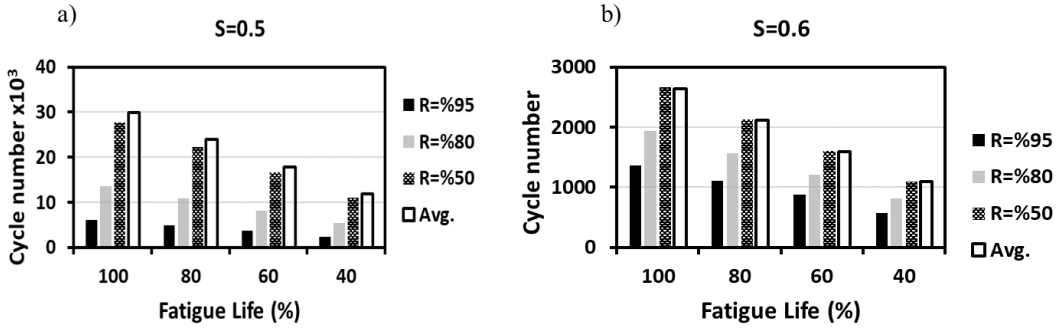

Figure 4.21. *The comparison of cycle numbers at 95%, 80%, and 50% Weibull Reliability for a) S=0.5 and b) S=0.6*

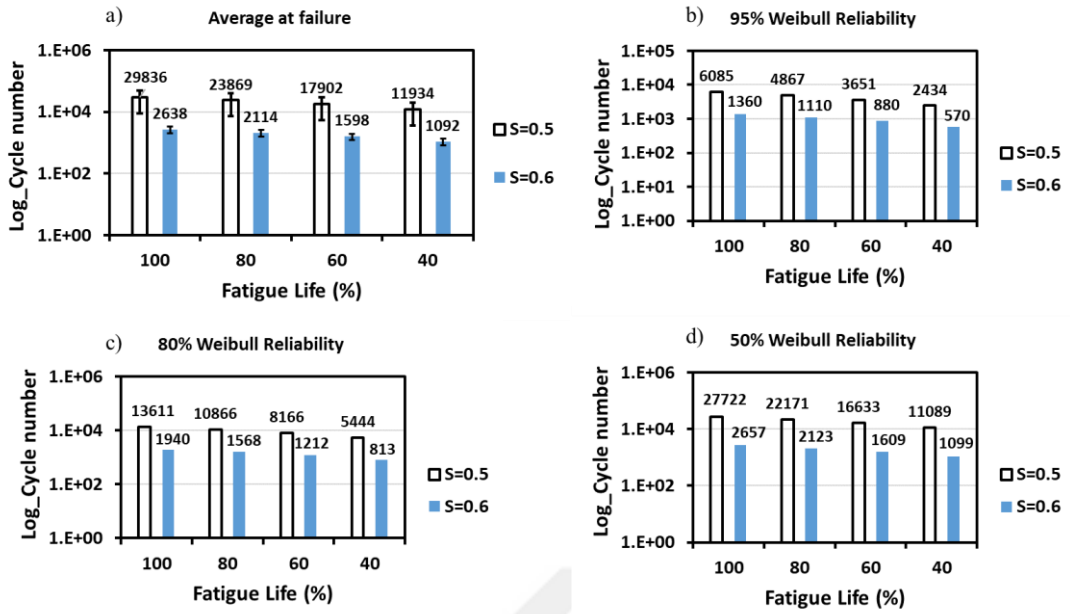

Figure 4.22. *a) Average cycle numbers at failure and the cycle numbers at b) 95%, c) 80%, and d) 50% reliability for different stress amplitudes (S)*

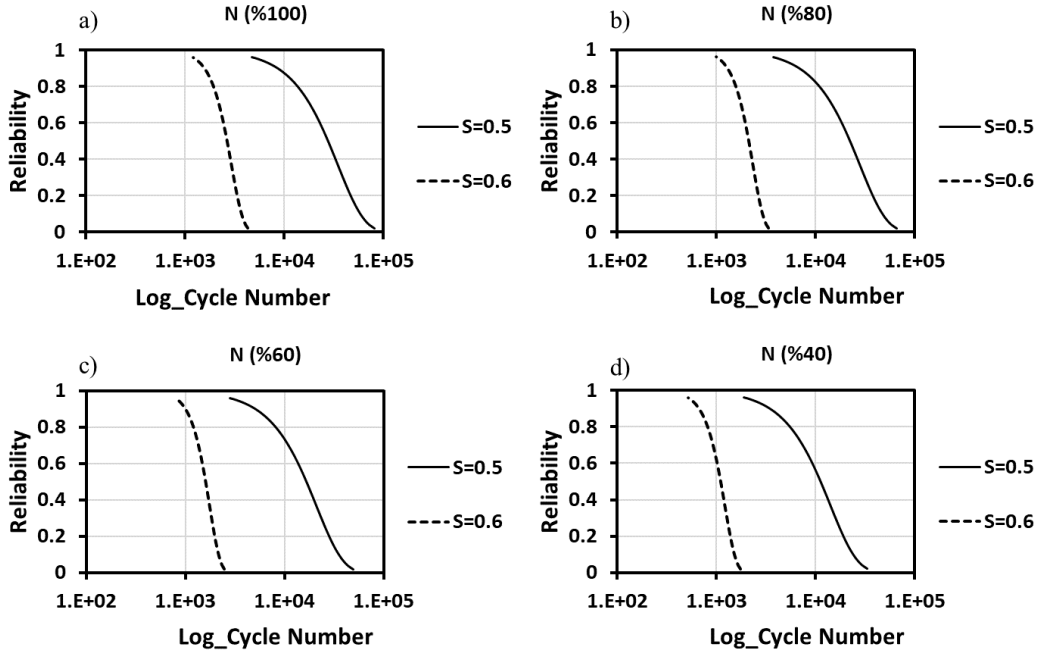

Figure 4.23. *Reliability curves based on the cycle number for a) N=100%, b) N=80%, c) N=60%, and d) N=40%*

4.8. Weibull Reliability for Electrical Resistance Change

Figure 4.24 compares the electrical resistance change values extracted from Tables 4.18 and 4.19 to better illustrate the effect of the reliability on the electrical resistance change. The average and the 50% Weibull reliability values are approximately same as expected. It is seen that the higher reliability, the lower the resistance change in the

specimens at each fatigue life. This is an expected result because lower damage accumulation within the specimens at higher reliability results with the reduction in the electrical resistance change value. At both stress amplitudes, the discrepancy of the electrical resistance change values between different fatigue lifes is greater at the lower reliability. This result is mainly due to the fact that higher damage accumulation at the lower reliability leads to significant change in the electrical resistance. However, the damage level at the higher reliability is very low resulting with lower electrical resistance change and ensuring the structural integrity at high reliability. Figure 4.25 also compares the cycle number values to emphasize the effect of the stress amplitude on the electrical resistance change. The electrical resistance change values at the stress amplitude of S=0.6 for each fatigue life are higher than that of the S=0.5. For the stress amplitudes of S=0.6 and S=0.5 at 100% fatigue life, electrical resistance change with 95% reliability were observed as 23% and 64%, respectively. Figure 4.26 displays graphs of reliability-cycle number curves comparatively for two different stress amplitudes. It is seen that the cycle number of S=0.5 is greater than that of S=0.6 at all reliability and fatigue life.

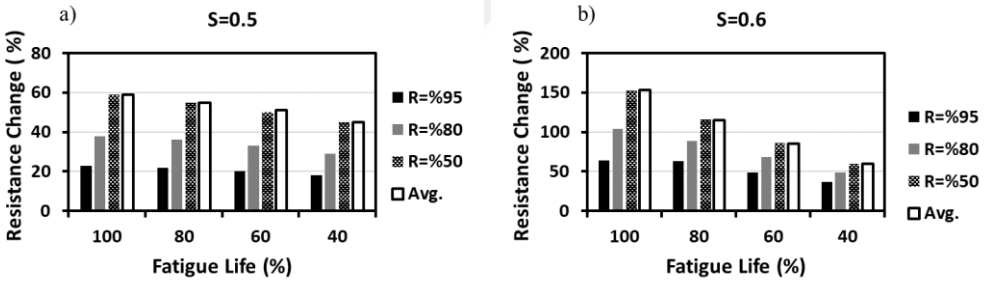

Figure 4.24. *The comparison of electrical resistance change at 95%, 80%, and 50% Weibull Reliability for a) S=0.5 and b) S=0.6*

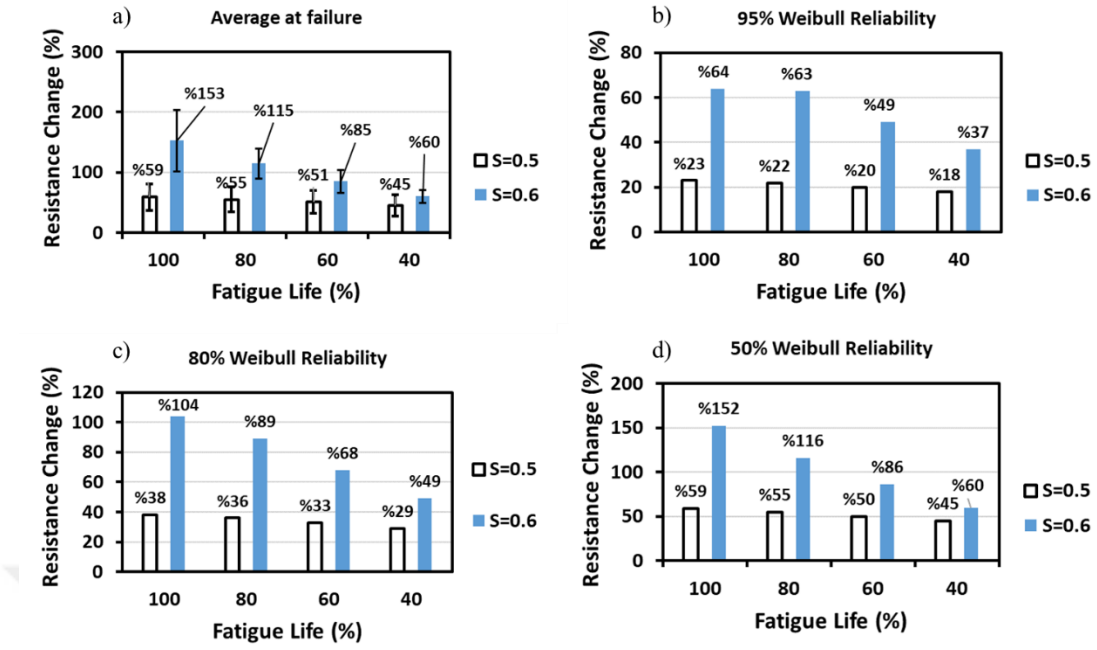

Figure 4.25. *a) Average electrical resistance changes at failure and the electrical resistance changes at b) 95%, c) 80%, and d) 50% reliability for different stress amplitudes (S)*

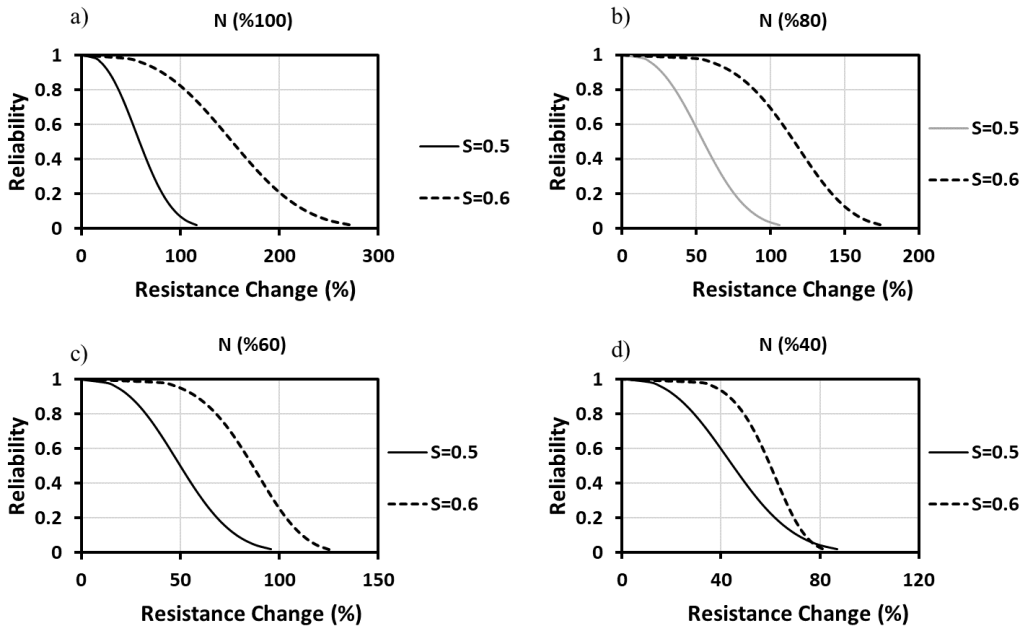

Figure 4.26. *Reliability curves based on the cycle number for a) N=100%, b) N=80%, c) N=60%, and d) N=40%*

Tables 4.20. and 4.21 show the fatigue life and stiffness loss of each specimen corresponding to electrical resistance change at 95%, 80%, and 50% reliability for S=0.5 and S=0.6, respectively. The results indicate that the stiffness loss and fatigue life increase along with the reduction in reliability. The average stiffness losses are seen as 12.2%, 16.2%, and 20.8 at the electrical resistance change corresponding to the 95%, 80%, and

50% Weibull reliability, respectively for S=0.5. In addition, the average fatigue lifes at the electrical resistance changes corresponding to the 95%, 80%, and 50% Weibull reliability are observed as 14.4%, 40.4%, and 81.8% for S=0.5. Similarly, the average stiffness losses are seen as 17.6%, 21.6%, and 24.2 at the electrical resistance change corresponding to the 95%, 80%, and 50% Weibull reliability, respectively for S=0.6. Also, the average fatigue lifes at the electrical resistance changes corresponding to the 95%, 80%, and 50% Weibull reliability are observed as 45.4%, 74.2%, and 94.4% for S=0.6.

Table 4.20. *The fatigue life and stiffness loss at 95%, 80%, and 50% reliability for S=0.5*

Stress Amplitude	Specimen No	ΔR (%95)=%23		ΔR (%80)=%38		ΔR (%50)=%59	
		N (%)	E_{loss} (%)	N (%)	E_{loss} (%)	N (%)	E_{loss} (%)
S=0.5	1	16	9	25	11	96	19
	2	14	13	40	19	100	24
	3	29	19	100	22	100	22
	4	10	10	32	16	100	22
	5	3	10	5	13	13	17
Average		14.4	12.2	40.4	16.2	81.8	20.8

Table 4.21. *The fatigue life and stiffness loss at 95%, 80%, and 50% reliability for S=0.6*

Stress Amplitude	Specimen No	ΔR (%95)=%64		ΔR (%80)=%104		ΔR (%50)=%153	
		N (%)	E_{loss} (%)	N (%)	E_{loss} (%)	N (%)	E_{loss} (%)
S=0.6	1	43	13	67	17	83	21
	2	49	16	76	20	99	24
	3	60	17	100	24	100	24
	4	35	19	53	21	90	24
	5	40	23	75	26	100	28
Average		45.4	17.6	74.2	21.6	94.4	24.2

5. CONCLUSION

The study examines how the electrical resistance of GFRP composites changes under fatigue loading at two different stress amplitudes, specifically S=0.6 and S=0.5. To guarantee electrical conductivity in GFRP composites, 0.3 wt% of MWCNTs were dispersed within the epoxy matrix using ultrasonication. Throughout the fatigue tests, electrical resistance measurements were concurrently conducted to monitor damage. Ultimately, an analysis using a two-parameter Weibull distribution was performed to establish reliability curves for predicting fatigue failure based on the electrical resistance change ratio.

The fatigue test data indicates a higher stiffness loss of 28% at S=0.6 compared to a stiffness loss of 25% at S=0.5, indicating a faster degradation of the material at higher stress amplitudes. The electrical resistance change curves demonstrate that damage accumulation leads to an increased resistance due to the growing disruption of conductive CNT networks within the composites. Consistent resistance change characteristics at the same stress amplitude suggest a reliable sensing technique. However, the average resistance change ratio at failure was found to be 153% for S=0.6 and 59% for S=0.5, indicating a dependency of electrical resistance change behavior on stress amplitude. Moreover, the response of resistance change to damage accumulation is more prominent than the observed stiffness loss.

The electrical resistance change ratio decreases with increasing reliability, attributed to lower damage accumulation. Consequently, a higher electrical resistance change ratio at greater reliability ensures more effective preservation of the structural integrity of GFRP composites. The scattering level of the electrical resistance change ratio between different fatigue life increases with the increase in the reliability. Substantial damage accumulation, associated with higher reliability, causes significant disruption in the conductive CNT networks, resulting in a considerable disparity in the electrical resistance ratio. For a 95% higher reliability, the electrical resistance change ratios at failure were determined to be 23% and 64% for S=0.6 and S=0.5, respectively. However, the difference in electrical resistance change ratios between the two stress amplitudes tends to diminish for lower fatigue life due to less damage accumulation leading to fewer disruptive changes in CNT networks during the early stages of damage accumulation. The impact of stress amplitude on the Weibull reliability of the electrical resistance change ratio is apparent. The average stiffness losses were found to be 12.2%,

16.2%, and 20.8% at the electrical resistance change corresponding to 95%, 80%, and 50% Weibull reliability, respectively, for S=0.5. The residual life were observed as 85.6%, 59.6%, and 18.2% at the electrical resistance change corresponding to 95%, 80%, and 50% Weibull reliability, respectively, for S=0.5. These trends were more pronounced at S=0.6 due to a higher rate of damage accumulation.

The successful application of electrical resistance change method to monitor the fatigue damage level of GFRP composites at two different stress amplitudes was demonstrated throughout this thesis. As a future work, the effect of the CNT content on the electrical resistance change behavior of FRP composites can be studied. In addition, high cycle fatigue tests corresponding to the low stress amplitudes should be investigated to better emphasize the effect of the stress amplitude on the electrical resistance change behavior. It should also be noted that the specimen number has an important effect on the Weibull distribution and therefore more trials of fatigue tests should be conducted for the purpose of determining preventative electrical resistance change ratio.

REFERENCES

Abot, J. L., Song, Y., Vatsavaya, M. S., Medikonda, S., Kier, Z., Jayasinghe, C., Rooy, N., Shanov, V. N., & Schulz, M. J. (2010). Delamination detection with carbon nanotube thread in self-sensing composite materials. *Composites Science and Technology*, *70*(7), 1113–1119. https://doi.org/10.1016/j.compscitech.2010.02.022

Arronche, L., La Saponara, V., Yesil, S., & Bayram, G. (2013). Impact damage sensing of multiscale composites through epoxy matrix containing carbon nanotubes. *Journal of Applied Polymer Science*, *128*(5), 2797–2806. https://doi.org/10.1002/app.38448

Böger, L., Sumfleth, J., Hedemann, H., & Schulte, K. (2010). Improvement of fatigue life by incorporation of nanoparticles in glass fibre reinforced epoxy. *Composites Part A: Applied Science and Manufacturing*, *41*(10), 1419–1424. https://doi.org/10.1016/j.compositesa.2010.06.002

Brasington, A., Sacco, C., Halbritter, J., Wehbe, R., & Harik, R. (2021). Automated fiber placement: A review of history, current technologies, and future paths forward. *Composites Part C: Open Access*, *6*, 100182. https://doi.org/10.1016/j.jcomc.2021.100182

Castillo, E., & Canteli, F. A. (2009). *A unified statistical methodology for modeling fatigue damage*. Springer.

Daniel, I. M., & Ori Ishai. (2006). *Engineering Mechanics of Composite Materials* (2nd ed.). Oxford University Press.

Ding, J., & Cheng, L. (2021). Ultra-high three-point bending fatigue fracture characteristics of CFRP modified by MWCNTs and fatigue life data analysis. *Composite Structures*, *259*. https://doi.org/10.1016/j.compstruct.2020.113468

Dresselhaus, M. S., Dresselhaus, G., & Saito, R. (1995). Physics of carbon nanotubes. *Carbon*, *33*(7), 883–891. https://doi.org/10.1016/0008-6223(95)00017-8

Ebbesen, T., & Ajayan, P. (1992). Large-scale synthesis of carbon nanotubes. *Letters to Nature*, *358*, 220–222.

Foundation, A., Blaedel, W. J., Wang, J., Rochon, A. M., Gesser, H. D., Aubert, J. H., Rand, P. B., Arnold, C., Clough, L. R., Clough, R. L., Guyomar, P. Y., Astruc, M., Wang, J., Hucke, E. E., Soffer, A., Astruc, M., Dubreuil, J. P., Lu, K. L., Lago, R. M., … Catalysis, T. (1996). Mechanical Damage of Carbon Nanotubes by Ultrasound. *Carbon*, *34*(6), 814–816.

Gao, L., Chou, T. W., Thostenson, E. T., Zhang, Z., & Coulaud, M. (2011). In situ sensing of impact damage in epoxy/glass fiber composites using percolating carbon nanotube networks. In *Carbon* (Vol. 49, Issue 10, pp. 3382–3385). Elsevier Ltd. https://doi.org/10.1016/j.carbon.2011.04.003

Gao, L., Thostenson, E. T., Zhang, Z., Byun, J. H., & Chou, T. W. (2010). Damage monitoring in fiber-reinforced composites under fatigue loading using carbon

nanotube networks. *Philosophical Magazine*, *90*(31–32), 4085–4099. https://doi.org/10.1080/14786430903352649

Gao, L., Thostenson, E. T., Zhang, Z., & Chou, T. (2009a). Sensing of Damage Mechanisms in Fiber-Reinforced Composites under Cyclic Loading using Carbon Nanotubes. *Advanced Functional Materials*, *19*(1), 123–130. https://doi.org/10.1002/adfm.200800865

Gao, L., Thostenson, E. T., Zhang, Z., & Chou, T. W. (2009b). Coupled carbon nanotube network and acoustic emission monitoring for sensing of damage development in composites. *Carbon*, *47*(5), 1381–1388. https://doi.org/10.1016/j.carbon.2009.01.030

Gupta, M., Jain, A., Kamineni, J. N., & Burela, R. G. (2022). Advances and applications of biofiber-based polymer composites. In *Advances in Bio-Based Fiber* (pp. 575–602). Elsevier. https://doi.org/10.1016/B978-0-12-824543-9.00002-5

Hamada, N., Sawada, S. I., & Oshiyama, A. (1992). New one-dimensional conductors: Graphitic microtubules. *Physical Review Letters*, *68*(10), 1579–1581. https://doi.org/10.1103/PhysRevLett.68.1579

Harris, B. (2003). *Fatigue in composites*. CRC Press.

Hwang, W., & Han, K. S. (1986). Fatigue of Composites—Fatigue Modulus Concept and Life Prediction. *Journal of Composite Materials*, *20*(2), 154–165. https://doi.org/10.1177/002199838602000203

Joshi, S. C. (2012). The pultrusion process for polymer matrix composites. In *Manufacturing Techniques for Polymer Matrix Composites (PMCs)* (pp. 381–413). Elsevier. https://doi.org/10.1533/9780857096258.3.381

Loyola, B. R., Briggs, T. M., Arronche, L., Loh, K. J., La Saponara, V., O'Bryan, G., & Skinner, J. L. (2013). Detection of spatially distributed damage in fiber-reinforced polymer composites. *Structural Health Monitoring*, *12*(3), 225–239. https://doi.org/10.1177/1475921713479642

Mallick, P. K. (2021a). Thermoset matrix composites for lightweight automotive structures. In *Materials, Design and Manufacturing for Lightweight Vehicles* (pp. 229–263). Elsevier. https://doi.org/10.1016/B978-0-12-818712-8.00006-9

Mallick, P. K. (2021b). Thermoset matrix composites for lightweight automotive structures. In *Materials, Design and Manufacturing for Lightweight Vehicles* (pp. 229–263). Elsevier. https://doi.org/10.1016/B978-0-12-818712-8.00006-9

Mallick, P. K. (2021c). Thermoset matrix composites for lightweight automotive structures. In *Materials, Design and Manufacturing for Lightweight Vehicles* (pp. 229–263). Elsevier. https://doi.org/10.1016/B978-0-12-818712-8.00006-9

Mantell, S. C., & Springer, G. S. (1994). Filament winding process models. *Composite Structures*, *27*(1–2), 141–147. https://doi.org/10.1016/0263-8223(94)90075-2

Markus Sause. (2010). *Identification of failure mechanisms in hybrid materials utilizing pattern recognition techniques applied to acoustic emission signals*. University of Augsburg.

Mayuet, P. F., Girot, F., Lamíkiz, A., Fernández-Vidal, S. R., Salguero, J., & Marcos, M. (2015). SOM/SEM based Characterization of Internal Delaminations of CFRP Samples Machined by AWJM. *Procedia Engineering*, *132*, 693–700. https://doi.org/10.1016/j.proeng.2015.12.549

Mazela, B., Batista, A., & Grześkowiak, W. (2020). Expandable Graphite as a Fire Retardant for Cellulosic Materials—A Review. *Forests*, *11*(7), 755. https://doi.org/10.3390/f11070755

Monti, M., Natali, M., Petrucci, R., Kenny, J. M., & Torre, L. (2011). Carbon nanofibers for strain and impact damage sensing in glass fiber reinforced composites based on an unsaturated polyester resin. *Polymer Composites*, *32*(5), 766–775. https://doi.org/10.1002/pc.21098

Mostafa, N. H., Ismarrubie, Z. N., Sapuan, S. M., & Sultan, M. T. H. (2017). Fibre prestressed polymer-matrix composites: A review. In *Journal of Composite Materials* (Vol. 51, Issue 1, pp. 39–66). SAGE Publications Ltd. https://doi.org/10.1177/0021998316637906

Naghashpour, A., & Van Hoa, S. (2013). A technique for real-time detection, location and quantification of damage in large polymer composite structures made of electrically non-conductive fibers and carbon nanotube networks. *Nanotechnology*, *24*(45), 455502. https://doi.org/10.1088/0957-4484/24/45/455502

Prakash, R. (1980). Non-Destructive Testing of Composites. *Composites*, *11*(4), 217–224. https://doi.org/10.1016/0010-4361(80)90428-0

Raulo, A., Suin, S., Paria, S., & Khatua, B. B. (2016). Expanded graphite (EG) as a potential filler in the reduction of percolation threshold of multiwall carbon nanotubes (MWCNT) in the PMMA/HDPE/EG/MWCNT nanocomposites. *Polymer Composites*, *37*(7), 2070–2082. https://doi.org/10.1002/pc.23385

Razali, N., Mansor, M. R., Omar, G., Kamarulzaman, S. A. F. S., Zin, M. H., & Razali, N. (2021). Out-of-autoclave as a sustainable composites manufacturing process for aerospace applications. In *Design for Sustainability* (pp. 395–413). Elsevier. https://doi.org/10.1016/B978-0-12-819482-9.00011-3

Reifsnider, K. L. (1991). *Fatigue of composite materials*. Elsevier.

Sakin, R., & Ay, I. (2008a). Statistical analysis of bending fatigue life data using Weibull distribution in glass-fiber reinforced polyester composites. *Materials and Design*, *29*(6), 1170–1181. https://doi.org/10.1016/j.matdes.2007.05.005

Sakin, R., & Ay, İ. (2008b). Statistical analysis of bending fatigue life data using Weibull distribution in glass-fiber reinforced polyester composites. *Materials & Design*, *29*(6), 1170–1181. https://doi.org/10.1016/j.matdes.2007.05.005

Spasojevic, P. M. (2019). Thermal and Rheological Properties of Unsaturated Polyester Resins-Based Composites. In *Unsaturated Polyester Resins* (pp. 367–406). Elsevier. https://doi.org/10.1016/B978-0-12-816129-6.00015-6

Strzelecki, P. (2021). Determination of fatigue life for low probability of failure for different stress levels using 3-parameter Weibull distribution. *International Journal of Fatigue*, *145*. https://doi.org/10.1016/j.ijfatigue.2020.106080

Thostenson, E. T., & Chou, T. W. (2006). Carbon nanotube networks: Sensing of distributed strain and damage for life prediction and self healing. *Advanced Materials*, *18*(21), 2837–2841. https://doi.org/10.1002/adma.200600977

Thostenson, E. T., & Chou, T. W. (2008). Real-time in situ sensing of damage evolution in advanced fiber composites using carbon nanotube networks. *Nanotechnology*, *19*(21). https://doi.org/10.1088/0957-4484/19/21/215713

Wang, J., Zhou, W., Guo, X., Su, M., & Ma, L. (2023). Effects of thermal aging on damage evolution behavior of glass fiber reinforced composites with multilayer graphene by acoustic emission. *Journal of Applied Polymer Science*, *140*(8). https://doi.org/10.1002/app.53524

Yesil, S., Winkelmann, C., Bayram, G., & La Saponara, V. (2010). Surfactant-modified multiscale composites for improved tensile fatigue and impact damage sensing. *Materials Science and Engineering: A*, *527*(27–28), 7340–7352. https://doi.org/10.1016/j.msea.2010.07.105

Zhang, H., Liu, Y., Kuwata, M., Bilotti, E., & Peijs, T. (2015). Improved fracture toughness and integrated damage sensing capability by spray coated CNTs on carbon fibre prepreg. *Composites Part A: Applied Science and Manufacturing*, *70*, 102–110. https://doi.org/10.1016/j.compositesa.2014.11.029

CURRICULUM VITAE

ORCID ID: 0009-0003-5750-0014

Name Surname : Ömer Keskin

Foreign Language : English

Education and Professional Background:

- 2017, Eskisehir Osmangazi University Faculty of Engineering and Architecture, Mechanical Engineering